nature metabolism

Article

https://doi.org/10.1038/s42255-025-01399-3

Glycerol-3-phosphate activates ChREBP, FGF21 transcription and lipogenesis in citrin deficiency

Received: 23 January 2025

Accepted: 29 September 2025

Published online: 14 November 2025

Check for updates

Vinod Tiwari[1], Byungchang Jin[2], Olivia Sun[1], Edwin D. J. Lopez Gonzalez[1], Min-Hsuan Chen[1], Xiwei Wu[1], Hardik Shah[3], Andrew Zhang[2], Mark A. Herman[4], Cassandra N. Spracklen[5], Russell P. Goodman[2] & Charles Brenner[1]

Citrin deficiency (CD) is caused by the inactivation of SLC25A13, a mitochondrial membrane protein required to move electrons from cytosolic NADH to the mitochondrial matrix in hepatocytes. People with CD do not like sweets. Here we show that SLC25A13 loss causes the accumulation of glycerol-3-phosphate (G3P), which activates the carbohydrate response element-binding protein (ChREBP) to transcribe FGF21, which acts in the brain to restrain intake of sweets and alcohol and to transcribe key genes driving lipogenesis. Mouse and human data suggest that G3P–ChREBP is a mechanistic component of the Randle Cycle that contributes to metabolic-dysfunction-associated steatotic liver disease and forms part of a system that communicates metabolic states from the liver to the brain in a manner that alters food and alcohol choices. The data provide a framework for understanding FGF21 induction in varied conditions, suggest ways to develop FGF21-inducing drugs and suggest potential drug candidates for lean metabolic-dysfunction-associated steatotic liver disease and support of urea cycle function in CD.

Citrin deficiency (CD) is an autosomal recessive disease caused by mutation of the citrin gene, *SLC25A13*, which encodes a mitochondrial membrane protein highly expressed in hepatocytes with a key role in moving high energy electrons from the cytosol to the mitochondrial matrix[1,2]. Infants with CD are diagnosed in their first month with jaundice and elevated circulation of ammonia, citrulline and arginine, resembling a urea cycle disorder[3], coincident with elevated lactate, resembling a mitochondrial disease[4]. Though CD is panethnic[5], it is most frequently diagnosed in the Far East. Data indicate a pathological allele frequency of up to 1 in 28 in southern China, 1 in 45 across other parts of China[6] and 1 in 50–100 elsewhere in the Far East[7]. CD is underdiagnosed outside of the Far East[8] with a global disease burden that remains not well calculated and with unknown effects for *SLC25A13*-mutation carriers.

By weight, carbohydrates constitute the largest class of macronutrient in human breast milk[9] such that infant livers are primed to use carbohydrates as fuel, which requires nicotinamide adenine dinucleotide (NAD) coenzymes in the hydride-accepting NAD^+ form in both the cytosol and the mitochondrial matrix[10]. As shown in Fig. 1a, glycolysis yields pyruvate and NADH in the cytosol. Whereas pyruvate can be transported to the mitochondrial matrix for further oxidation[11], cytosolic NADH does not cross the mitochondrial membrane[12]. Rather, the high energy electrons—termed reducing equivalents—picked up by NAD^+ are moved to mitochondrial electron transport by two major

[1]Beckman Research Institute of City of Hope, Duarte, CA, USA. [2]Liver Center and Endocrine Unit, Massachusetts General Hospital, Boston, MA, USA. [3]Comprehensive Cancer Center, University of Chicago, Chicago, IL, USA. [4]Baylor College of Medicine, Houston, TX, USA. [5]Department of Biostatistics and Epidemiology, University of Massachusetts, Amherst, MA, USA. e-mail: cbrenner@coh.org

NADH shuttle systems, the malate–aspartate (Asp) shuttle (MAS)[13] and the glycerol-3-phosphate (G3P) dehydrogenase shuttle (GPDS)[14]. In hepatocytes, SLC25A13 is the component of the MAS that mediates Asp entry into cytosol in exchange for glutamate (Glu) transport into the mitochondrial matrix[15]. Another Glu/Asp antiporter encoded by SLC25A12 has higher expression in brain and muscle—its expression in hepatocytes is considered a primary mechanism of disease modification and/or escape in CD[16].

The resemblance of CD to a mitochondrial disease can be explained by failure of CD hepatocytes to obtain mitochondrial energy from complete oxidation of carbohydrates, with elevated lactate being an expected outcome of elevated cytosolic NADH. The resemblance of CD to a urea cycle disorder can be explained by a deficiency in hepatocytosolic Asp, which is required for the citrulline-consuming step of the urea cycle[5]. After diagnosis, children with CD, classified as cases of neonatal intrahepatic cholestasis caused by CD[2,3], are managed nutritionally with a diet in which carbohydrates are largely replaced by medium chain triglycerides (MCTs)[5]. In most cases, neonatal intrahepatic cholestasis caused by CD goes into remission, and people with CD are able to grow and lead relatively normal lives, though they do not like sweets[3,17] and are prone to metabolic-dysfunction-associated steatotic liver disease (MASLD) despite a lean body mass[18]. In other cases, there is a failure to thrive with dyslipidemia caused by CD. In adulthood, CD symptomology can reactivate with diagnoses of adult-onset type II citrullinemia or adult-onset CD, which are characterized by hyperammonaemia, MASLD, pancreatitis and neuropsychiatric complications[2,3]. The conventional nutritional management of hyperammonaemia, that is, a lower protein, higher carbohydrate diet, does not benefit patients with CD[19].

When *Slc25a13* was knocked out in mice, there was no clear physiological phenotype[20]. Reasoning that the GPDS is more highly expressed in mouse liver than in human liver, researchers proceeded to inactivate the GPDS component *Gpd2*. Mice homozygous for the disruption of *Slc25a13* and *Gpd2* formed an excellent CD model, exhibiting hyperlactataemia, hyperammonaemia, hyperargininemia, hypercitrullinemia and MASLD[14]. When provided a choice between water and saccharine, $Slc25a13^{-/-}Gpd2^{-/-}$ mice behaved similarly to wild-type mice, choosing saccharine by a wide margin, indicating that there is no defect in detection of or desire for sweet taste in naive mice with an inactivation of the two NADH shuttle systems[21]. However, when provided with a choice between sucrose and water, $Slc25a13^{-/-}Gpd2^{-/-}$ double mutants fail to prefer sucrose, suggesting that incomplete carbohydrate oxidation is required to produce the carbohydrate-aversive phenotype. Though wild-type mice consumed greater than 15 g of sucrose or 3 g of ethanol or 4 g of glycerol per 25-g mouse per day, $Slc25a13^{-/-}Gpd2^{-/-}$ double mutants had impaired preferences for sucrose, ethanol and glycerol when given a choice between water and these energy-containing liquids[21]. Single homozygous mutants in the MAS component *Slc25a13* and the GPDS component *Gpd2* generally had intermediate phenotypes. Metabolomic analysis showed the accumulation of glycerol and G3P in $Slc25a13^{-/-}Gpd2^{-/-}$ double mutants[21]. These data suggested that loss of the MAS and GPDS coupled with the provision of specific macronutrients result in a type of metabolic stress that leads to a behavioural change to avoid these compounds.

Fibroblast growth factor 21 (FGF21) is a secreted polypeptide made in the liver, adipose and muscle in response to a wide variety of stress conditions[22]. FGF21 has multiple sites of action including specific β-klotho-expressing regions of the brain, where FGF21 functions to restrain the intake of sweets[23] and ethanol[24], and the periphery, where it increases energy expenditure[25] and body temperature[26]. FGF21 was first termed a starvation hormone because it is released into circulation by the liver in response to fasting[27,28] and ketogenic diet (KD)[29] in mice. Though these conditions result in the release of free fatty acids, which activate PPARα function at peroxisome proliferator response elements[30] in the *FGF21* promoter, the deletion of PPARα from mouse liver did not completely eliminate the induction of FGF21 by KD[29].

Literature on FGF21 induction is considered paradoxical[31] because FGF21 is not only induced by fasting and the near absence of dietary carbohydrates but also induced by the provision of simple carbohydrates[32–34], particularly fructose[35,36]. Moreover, in addition to being induced by fasting[27,28,37] and exercise[38,39], FGF21 is induced by refeeding[40], obesity[41], type 2 diabetes[42] and mitochondrial disease[43]. It has also been shown that FGF21 is induced by a loss-of-function variant of glucokinase regulator *GCKR*[44] and ethanol[45] via reductive stress, that is, conditions that increase the NADH/NAD^+ ratio in hepatocytes[46], and by protein restriction[47].

We considered whether mitochondrial disease, NADH shuttle disruption, ethanol, fructolysis and the conditions involving lipolysis, that is, fasting and exercise, might produce a common metabolite that would activate FGF21 transcription. As shown in Fig. 1b, we reasoned that mitochondrial disease, NADH shuttle disruption, elevated glycaemia and/or ethanol metabolism would elevate cytosolic NADH, leading to a buildup of G3P at the expense of dihydroxyacetone phosphate (DHAP). As shown in Fig. 1c, we reasoned that fructolysis could also lead to a buildup of G3P with G3P formed from DHAP and from glyceraldehyde. Finally, as shown in Fig. 1d, we reasoned that triglyceride lipolysis would produce glycerol and, consequently, G3P due to the activity of glycerol kinase.

Two of the key transcription factors acting within the *FGF21* promoter are PPARα and carbohydrate response element-binding protein (ChREBP)[31,34]. Although it is clear that PPARα strongly contributes to turning on FGF21 in conditions of fasting[27–29] and that FGF21 is both upstream and downstream of PPARα in the adaptive response to starvation[28], the PPARα-independent component of FGF21 induction in mice fed a KD[29] suggested the action of a different metabolite-sensing factor.

ChREBP, encoded by the *MLXIPL* gene, is a member of the MYC and MAX superfamily of heterodimerizing helix–loop–helix transcription factors that is abundantly expressed in the liver[48–50]. As a heterodimer with MAX-like protein X (MLX) and at elevated levels of glucose metabolites, ChREBP activates the transcription of target promoters containing carbohydrate response elements (ChoREs)[51]. Well-characterized ChoREs drive the ChREBP-dependent transcription of ChREBPβ—a shorter, carbohydrate-induced form of ChREBP[52], liver pyruvate kinase (*PKLR*)[53], *FGF21*[31] and other genes that are important for carbohydrate adaptations including those for de novo lipogenesis[51] such as Ac-coA lysase (*ACLY*), Ac-coA carboxylase (*ACACA*) and fatty acid synthetase (*FASN*).

In the extensive literature on ChREBP[48–50], researchers have reported that ChREBP is activated by a glucose metabolite that engages the N-terminal glucose-sensing module (GSM)[54], which is conserved between ChREBP and the related MondoA transcription factor[55]. The specific identity of this metabolite remains less clear, however, as evidence has been presented for glucose-6-phosphate (G6P)[55,56], fructose-2-6-bisphosphate (F2,6BP)[57] and xylulose-5-phosphate (X5P)[58]. It is difficult to distinguish between these proposed mechanisms because typical ChREBP activation conditions involve a shift from low glucose to high glucose that would simultaneously elevate all proposed ChREBP GSM-activating ligands, and none of these metabolites have been shown directly to bind the GSM. Moreover, it is challenging to reconcile the previously proposed ChREBP ligands with data showing that glycerol treatment strongly activates hepatic ChREBP in vivo[59].

Recent work has shown that the key transcription factor for the ethanol induction of FGF21 is ChREBP and that the ChREBP transcription programme is downstream of an increase in the NADH/NAD^+ ratio that occurred with a rise in a select group of metabolites that include G3P but not G6P or X5P[60]. We hypothesize that patients with CD and mouse models have a sweet- and ethanol-aversive phenotype because their livers activate a G3P–ChREBP–FGF21 transcription programme (Fig. 1b). Moreover, we suggest that this mechanism resolves what have been considered paradoxical aspects of FGF21 induction because

https://doi.org/10.1038/s42255-025-01399-3

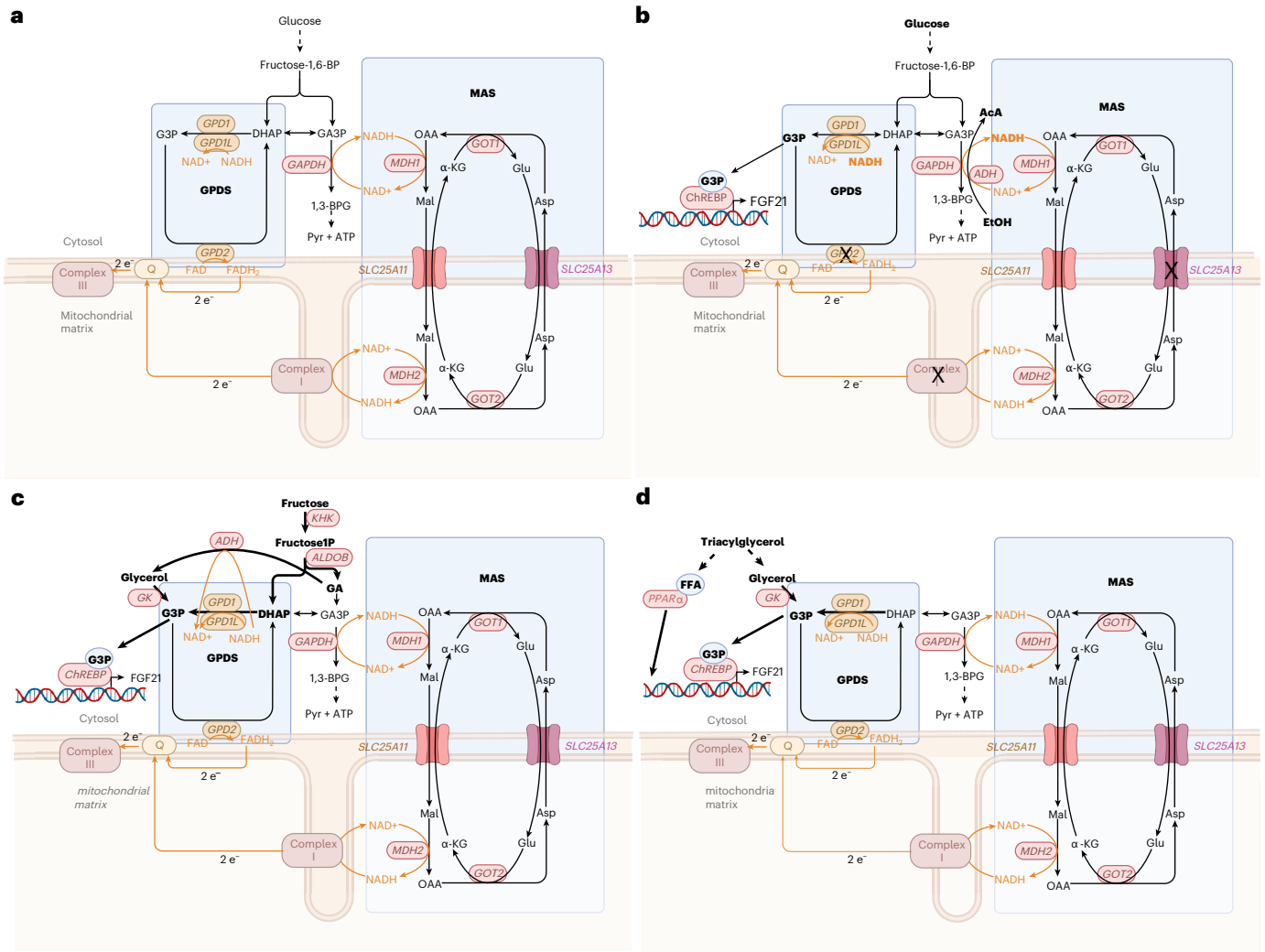

Fig. 1 | Inductive reasoning of a G3P–ChREBP–FGF21 transcription system in hepatocytes. FGF21 is induced in a wide variety of conditions that have eluded a unified theory of induction. The following diagrams of metabolite flow in hepatocytes as affected by conditions of metabolic stress led us to propose G3P as the activator of ChREBP that can resolve the paradoxes of FGF21. **a**, The metabolic flow in unperturbed hepatocytes is facilitated by two NADH shuttles without the induction of FGF21. The MAS[1] facilitates the transfer of reducing equivalents from cytosolic NADH to oxaloacetate, transiently forming malate, which is reoxidized at complex I in the mitochondrial matrix. The GPDS[13] facilitates the transfer of reducing equivalents from cytosolic NADH to DHAP, transiently forming G3P with reducing equivalents transferred to FAD, forming $FADH_2$, which is reoxidized with electron transfer to coenzyme Q in the mitochondrial electron transfer chain (METC). **b**, With either mitochondrial insufficiency, disruption of the MAS in CD, disruption of the GPDS, ethanol metabolism or elevated glucose, cytosolic NADH is expected to rise, which would be expected to cause the accumulation of G3P, which we propose to be the activator of ChREBP, driving the FGF21 expression. **c**, Fructolysis is predicted to elevate G3P, with one G3P equivalent formed from DHAP and another formed from glyceraldehyde (GA) via the function of alcohol dehydrogenase (ADH) and glycerol kinase[107]. The resulting G3P is proposed as the activating ligand for ChREBP activation and FGF21 expression. **d**, Triglyceride lipolysis is expected to produce glycerol and free fatty acids. Conversion of glycerol to G3P is proposed to activate ChREBP, which would co-operate with free fatty-acid-activated PPARα to drive transcription of FGF21. OAA, oxaloacetate; α-KG, α-ketoglutarate; 1,3-BPG, 1-3-bisphosphoglycerate; FFA, free fatty acid. Figure created with BioRender.com.

fasting and refeeding, KD and simple carbohydrates, mitochondrial disease, ethanol and fructose all have direct paths to producing G3P (Fig. 1b–d).

Here, we show that G3P accumulates in the liver of the mouse model of CD and that ChREBP is activated in this model with the transcription of FGF21 and the activation of a lipogenic transcriptional programme. Our data further show that G3P is a specific ligand of the ChREBP GSM and suggest that features of the G3P–ChREBP activation mechanism can account for why fructose is more lipogenic than glucose, provide a unifying mechanism for non-alcoholic and alcoholic hepatic steatogenesis, resolve paradoxes of FGF21 expression, and explain key aspects of CD pathogenesis including lean MASLD, the favourable effects of MCTs and severe urea cycle dysfunction. This work suggests drug targets for treatment of CD, lean MASLD and common MASLD and also implicates CD mutation carriers, who number in the millions, as people with a distinct metabolic profile consistent with elevated circulation of FGF21.

Results

Deletion of NADH shuttle systems and provision of glycerol cause increased FGF21 circulation in mice

Sperm from C57BL/6J mice of genotype *Slc25a13*$^{-/-}$*Gpd2*$^{-/-}$ (ref. 21) were used for the in vitro fertilization of C57BL/6J females. Subsequent crosses generated male and female *Slc25a13*$^{-/-}$ mice, *Gpd2*$^{-/-}$ mice and,

https://doi.org/10.1038/s42255-025-01399-3

at much lower than Mendelian ratios, *Slc25a13*$^{-/-}$*Gpd2*$^{-/-}$ mice. Consistent with our first prediction, as shown in Fig. 2a, mice with deletion of either *Slc25a13* or *Gpd2* tended to have elevated circulating FGF21, whereas mice inactivated for both NADH shuttle systems had around threefold-elevated FGF21. This result was significant for mice of both sexes (Fig. 2a), for male mice (Fig. 2b) and for females (Fig. 2c). Mice of each genotype with 5% (w/v) glycerol in their drinking water for 2 days had significantly elevated circulating FGF21 by virtue of glycerol exposure, and the effects of genotype and glycerol were additive. The effect of glycerol on the induction of FGF21 was highly significant in each genotype irrespective of sex (Fig. 2a) and in males (Fig. 2b). Further, *Slc25a13*$^{-/-}$*Gpd2*$^{-/-}$ females have significantly higher circulating FGF21 than wild-types or either single mutant upon exposure to glycerol (Fig. 2c). Thus, consistent with the hypothesis that sweet aversion in CD is due to a G3P–ChREBP–FGF21 induction programme, the mouse model of CD overproduces FGF21 and superinduces FGF21 when exposed to glycerol.

Deletion of NADH shuttle systems and provision of glycerol activate hepatic ChREBP, FGF21 and lipogenic transcription

To determine whether the deletion of NADH shuttle systems and/or provision of glycerol result in a ChREBP transcriptional programme, we collected livers from 40 mice representing water- and glycerol-exposed males of the four genotypes, prepared complementary DNA (cDNA) and performed bulk paired-end 150 base-pair RNA sequencing (RNA-seq)[61] using an Illumina NovaSeq X Plus sequencer at >20 million paired reads per sample. As shown in Fig. 3, the ChREBP transcriptional programme is evident as judged by induction of well-characterized ChREBP target genes including *ChREBPβ*; *Fgf21*; *Pklr*; *Khk*, *Aldob* and *Tkfc* (the three key enzymes of fructolysis); *Gpi1* and *Pgd* (phosphoglucose isomerase and 6-phosphogluconate dehydrogenase); *Fasn*, *Elovl6* and *Agpat2* (key enzymes for triglyceride synthesis); and *Tm6sf2* (very low-density lipoprotein synthesis factor).

Many of the genes of de novo lipogenesis are dually activated by ChREBP and sterol response element-binding protein 1c (SREBP-1c)[62], encoded by the *Srebf1* gene. To test whether the mouse model of CD dysregulates either of these transcription factors and to examine the relationship with *Fgf21* expression, we calculated the levels of specific transcripts using RSEM[63]. As presented in Extended Data Table 1, *Srebf1* expression was unaffected by deletion of *Slc25a13* and/or *Gpd2* and was unaffected by addition of glycerol. The *ChREBPβ* transcript was induced by about 2.4-fold by glycerol in the wild-type strain, about 4.5-fold by loss of either of the NADH shuttle genes and nearly 13-fold by the inactivation of both genes. The *ChREBPα* transcript was largely unaffected by genotype but was induced approximately two- to threefold by glycerol in wild-type and single mutant strains. In the double mutant, which has the highest level of circulating FGF21 and the highest level of *ChREBPβ* transcript, there was no further induction of of *ChREBP* transcripts by glycerol. Consistent with the effect of FGF21 on feeding behaviours, at the mRNA level, glycerol induced *Fgf21* to a greater degree in the wild-type and *Slc25a13*$^{-/-}$ strains in which basal *Fgf21* expression was lowest and induced *Fgf21* the least in the *Gpd2*$^{-/-}$ and *Slc25a13*$^{-/-}$*Gpd2*$^{-/-}$ strains in which basal *Fgf21* expression was highest.

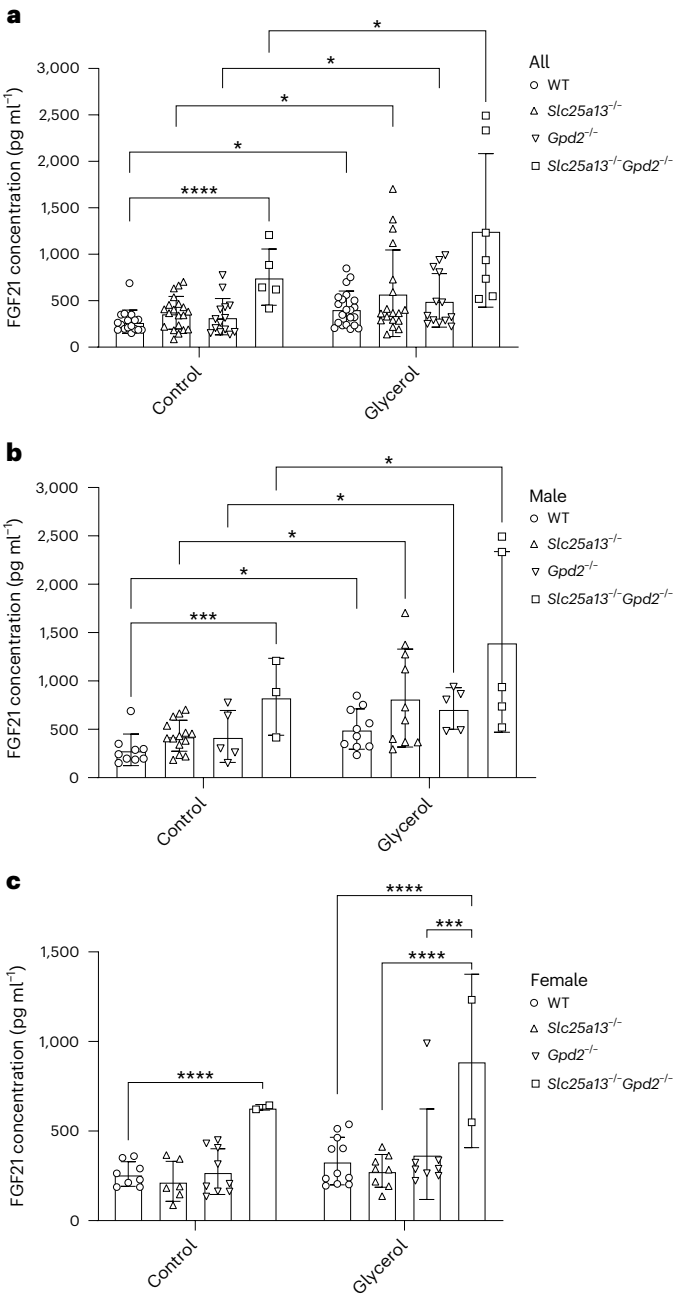

Fig. 2 | Inactivation of NADH shuttle systems and glycerol induce FGF21 circulation. a, The serum FGF21 from the mice of the indicated genotypes was measured after 2 days with ad libitim access to food and water. (Wild type is represented by circles, $n = 17$; *Slc25a13*$^{-/-}$ is represented by up triangles, $n = 20$; *Gpd2*$^{-/-}$ is represented by the down triangles, $n = 14$; *Slc25a*$^{-/-}$*Gpd2*$^{-/-}$ is represented by squares, $n = 5$). In parallel, additional mice were provided access to food and 5% (w/v) glycerol (wild type is represented by circles, $n = 21$; *Slc25a13*$^{-/-}$ is represented by up triangles, $n = 18$; *Gpd2*$^{-/-}$ is represented by down triangles, $n = 13$; *Slc25a*$^{-/-}$*Gpd2*$^{-/-}$ is represented by squares, $n = 7$). The data show that across both sexes, *Slc25a*$^{-/-}$*Gpd2*$^{-/-}$ mice have elevated FGF21 and that each genotype has its FGF21 circulation elevated by glycerol. **b**, Male subgroup analysis of food and water (wild type is represented by circles, $n = 9$; *Slc25a13*$^{-/-}$ is represented by up triangles, $n = 14$; *Gpd2*$^{-/-}$ is represented by the down triangles, $n = 5$; *Slc25a*$^{-/-}$*Gpd2*$^{-/-}$ is represented by squares, $n = 3$) or food and 5% (w/v) glycerol (wild type is represented by circles, $n = 10$; *Slc25a13*$^{-/-}$ is represented by up triangles, $n = 10$; *Gpd2*$^{-/-}$ is represented by down triangles, $n = 5$; *Slc25a*$^{-/-}$*Gpd2*$^{-/-}$ is represented by squares, $n = 5$). The data show that male *Slc25a*$^{-/-}$*Gpd2*$^{-/-}$ mice have elevated FGF21 and that each genotype has its FGF21 circulation elevated by glycerol. **c**, Female subgroup analysis of food and water (wild type is represented by circles, $n = 8$; *Slc25a13*$^{-/-}$ is represented by up triangles, $n = 6$; *Gpd2*$^{-/-}$ is represented by down triangles, $n = 9$; *Slc25a13*$^{-/-}$*Gpd2*$^{-/-}$ is represented by squares, $n = 2$) or food and 5% (w/v) glycerol (wild type is represented by circles, $n = 11$; *Slc25a13*$^{-/-}$ is represented by up triangles, $n = 8$; *Gpd2*$^{-/-}$ is represented by down triangles, $n = 8$; *Slc25a13*$^{-/-}$*Gpd2*$^{-/-}$ is represented by the squares, $n = 2$). The data show that female *Slc25a*$^{-/-}$*Gpd2*$^{-/-}$ mice have elevated FGF21 with respect to the wild type at baseline. In addition, the data show that female *Slc25a*$^{-/-}$*Gpd2*$^{-/-}$ mice have elevated FGF21 on glycerol with respect to each of the other genotypes on glycerol. Significant differences were calculated by applying two-way analysis of variance and Tukey's multiple comparisons test in which $^{*}P < 0.05$, $^{**}P < 0.005$, $^{***}P < 0.0005$ and $^{****}P < 0.0001$. The error bars represent means ± s.e.m. WT, wild type.

https://doi.org/10.1038/s42255-025-01399-3

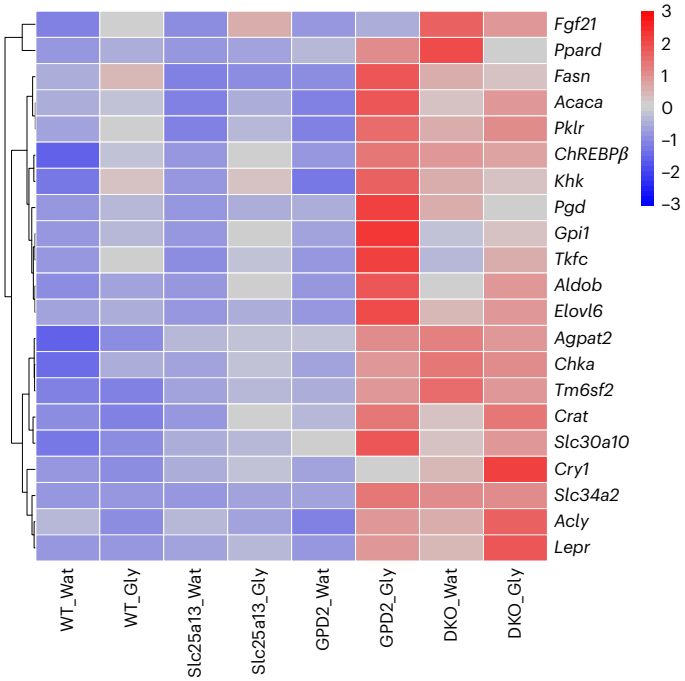

Fig. 3 | Inactivation of NADH shuttle systems and glycerol drive a ChREBP transcription programme. Hierarchical clustering of mean liver gene expression levels (fragments per kilobase of transcript per million mapped reads) of select ChREBP target genes across four genotypes of male mice exposed to either water (Wat) or glycerol (Gly). Experimental sample *n* numbers are provided in Table 1.

As the experiment was performed with 2 days of ad libitim access to 5% glycerol as the water source, and it has been shown that the CD mouse model has a sucrose, ethanol and glycerol-aversive phenotype[21], one would expect that the high basal levels of FGF21 in the *Slc25a13*$^{-/-}$*Gpd2*$^{-/-}$ strain significantly limit their glycerol intake and further increases in *Fgf21* mRNA expression.

Deletion of NADH shuttle systems result in accumulation of hepatic G3P

We performed targeted a metabolomic analysis of liver extracts from male mice of the four genotypes to determine whether G3P or compounds previously termed ChREBP activators accumulate as a function of NADH shuttle disruption. As shown in Fig. 4a, G3P was quantified at ~1 mM in livers from wild-type mice. The deletion of *Slc25a13*, *Gpd2* or both NADH shuttle genes resulted in levels of hepatic G3P that tended to be higher than levels of G3P in wild-type mouse livers. Similarly, the glycerol-exposed mouse livers of each of the four genotypes had levels of G3P that tended to be higher. On the basis that the ChREBPβ transcript is induced in *Slc25a13*$^{-/-}$, *Gpd2*$^{-/-}$ and *Slc25a13*$^{-/-}$*Gpd2*$^{-/-}$ mouse livers, we compared G3P levels in wild-type versus all mutant livers and observed a significant increase in G3P from 1.07 ± 0.20 mM to 1.95 ± 0.60 mM. As G6P[55,56], F2,6BP[57] and X5P[58] have been previously proposed to be activating ligands of ChREBP, we tested whether hexose phosphates or pentose phosphates were altered by conditions that activate ChREBP, namely glycerol and the deletion of NADH shuttle genes. As shown in Fig. 4c,d, the hepatic concentrations of hexose phosphates were not altered by genotype and/or addition of glycerol. As shown in Fig. 4e,f, relative levels of pentose phosphates were also unaffected. Thus, consistent with the proposed G3P–ChREBP–FGF21 activation mechanism in Fig. 1b and the observation that *Slc25a13*$^{-/-}$*Gpd2*$^{-/-}$ mice experiencing sweet- and ethanol-aversive behaviours have elevated hepatic G3P[21], we show that deletion of the NADH shuttle systems is sufficient specifically to elevate the proposed ChREBP-activating ligand.

Genetic manipulation of G3P drives ChREBP activation in a reconstituted system

HEK293T cells do not express ChREBP and show poor expression of MLX, thereby allowing the reconstitution of condition-dependent, ChREBP- and MLX-dependent, ChoRE-dependent transcription[60]. The robust ChoRE-luciferase activity in HEK293T cells depends on the introduction of both ChREBPα and MLX. The reconstituted transcriptional activity is depressed by the expression of *L. brevis* NADH oxidase (*Lb*NOX), which lowers the NADH/NAD$^+$ ratio, and increased by expression of *Escherichia coli* soluble transhydrogenase (*Ec*STH), an enzyme that uses reducing equivalents from NADPH to elevate the cytosolic NADH/NAD$^+$ ratio[60]. In prior work, this system was used to show that three metabolites, namely G3P, glyceraldehyde-3-phosphate (GA3P) and fructose-1,6-bisphosphate (F1,6BP), were highly correlated with ChREBPα activation but that levels of G6P and X5P were uncorrelated with ChREBP transcriptional activity[60]. To distinguish between potential ChREBPα-activating ligands, we introduced glycerol kinase (*GK*), *GPD1* and *GAPDH* genes into the reconstituted ChREBPα-MLX HEK293T system alongside green fluorescent protein (GFP), *Lb*NOX and *Ec*STH as inactive, ChoRE-luciferase-depressing and ChoRE-luciferase-activating controls, respectively. Though *GAPDH* had a minor ChoRE-luciferase depressing effect, and *GK* was without effect potentially due to the absence of a supply of glycerol, *GPD1* strongly increased ChoRE-luciferase activity (Fig. 5a). Relative quantification of 137 metabolites showed that in these cells, *GPD1* strongly depressed levels of GA3P and DHAP, while elevating G3P. The correlation coefficient (CC) for luciferase activity with relative G3P in the six resulting HEK293T transfected cell lines was 0.96 (Fig. 5b), exceeding all the other compounds tested (Supplementary Data). G6P (Fig. 5c), which has been considered a candidate ChREBP-activating ligand[55,56], was uncorrelated with ChoRE-luciferase activity (CC of −0.11). GA3P (Fig. 5d), which had appeared to be correlated to ChoRE-luciferase activity in prior work[60], became uncorrelated with inclusion of the effects of *GK*, *GPD1* and *GAPDH* (CC of 0.18).

To further map the site of G3P activity, we used the HEK293T system to characterize the sensitivity of ChREBPβ-MLX to altered levels of metabolites. As shown in Fig. 5e–g, ChREBPβ—the form of ChREBP without the N-terminal GSM[52]—was introduced into HEK293T cells and shown to induce ChoRE-luciferase in a manner that depends on MLX cotransfection. Moreover, ChoRE-luciferase activation from ChREBPβ-MLX was about threefold more potent than that from ChREBPα-MLX (Fig. 5h). However, when ChREBPβ-MLX-dependent ChoRE-luciferase was challenged by *Lb*NOX (Fig. 5i) and *Ec*STH (Fig. 5j) expression, there was no modulation of ChREBP transcriptional activity[60]. These data indicate that the metabolite that responds to an elevated NADH/NAD$^+$ ratio thereby driving ChREBP-MLX transcription[60] acts on the ChREBPα-specific N-terminus and is fully correlated with accumulation of G3P.

The GSM domain of ChREBP is a G3P-sensing module

Various constructs have been used to obtain structural or biophysical data on the GSM of ChREBP. Notably, a construct from residue 1 to 250 of mouse ChREBP was purified as a His-tagged protein in *E. coli* for structural characterization. However, this molecule was found to have been proteolyzed to a fragment of the GSM from residue 81 to 196 and, when mixed with the 14-3-3β protein for structural characterization, the full length of 14-3-3β and only residues 117–137 of ChREBP were structured[64]. Based on knowledge that both ChREBP and the homologous MondoA are responsive to glucose metabolites[54,65], we performed a careful multiple sequence alignment of ChREBP and MondoA and chose to define residues 43–307 of mouse ChREBP (ChREBP43–307) as a candidate stable, globular GSM.

After expression of His-tagged ChREBP43-307 in *E. coli* and purification by nickel nitrilotriacetic acid affinity chromatography, we characterized ligand binding by isothermal titration calorimetry[66].

Table 1 | The GSM of ChREBPα directly binds G3P

Ligand	K_d ± s.d. (μM)
G3P	17.0±1.1
G6P	64.3±13.5
F6P	131±43
X5P	164±16
GA3P	221±62
F1,6BP	250±37
Glucose	270±54
DHAP	453±31

Ligand affinities were determined in triplicate by isothermal titration calorimetry using a construct of purified mouse ChREBP GSM in which residues 43–307 were expressed carboxyl to $MetHis_6$. The data show that G3P is the highest-affinity ligand for the GSM. We suggest that hereafter the GSM be considered an abbreviation for G3P-sensing module.

As presented in Table 1, we tested glucose, G6P, F6P, F1,6BP, GA3P, DHAP, G3P and X5P for binding and were able to detect saturable binding with each ligand. However, the equilibrium dissociation constant (K_d) values for all but two ligands were greater than 130 μM. G6P, which has been considered a candidate GSM ligand[55,56] but is uncorrelated with ChREBP transcriptional activation[60] (Fig. 5c), showed half-saturated binding at 64.3 ± 13.5 μM, suggesting an association that could be displaced by a higher-affinity ligand whose abundance is sensitive to conditions that activate ChREBP. Indeed, G3P, which is greatly increased by the deletion of the NADH shuttle systems (Fig. 4) and GPD1 overexpression (Fig. 5a) and which correlates with ChREBP activation (Fig. 5B), binds the GSM with a K_d value of 17.0 ± 1.1 μM. Thus, biophysical, genetic, metabolomic and cellular reconstitution data indicate that the GSM of ChREBP should be termed a G3P-sensing module that drives the transcription of ChREBPβ, FGF21 and other ChREBP target genes. Notably, this model can account for the PPARα-independent induction of FGF21 in conditions of lipolysis[29]; for fructose and glycerol as activators of ChREBP[59]; and for ethanol[45], reductive stress[46], hyperglycaemia[42] and mitochondrial dysfunction[43] as drivers of FGF21 transcription.

After this work was available in preprint form[67], support for G3P as the activator of ChREBP was provided in an experiment in which reporter plasmid transcription from ChREBP and MLX was reconstituted in HEK293T cells and shown to increase in response to GPD1 overexpression[68] as we showed in Fig. 5a. Moreover, these investigators added G3P to HEK293T cells expressing ChREBP and MLX to show that the G3P addition protected ChREBP from thermal precipitation[68]. As all models of ChREBP activation depend on new protein interactions upon small molecule engagement[48,49], the cellular thermal denaturation assay does not constitute evidence for the direct binding of G3P. However, the work supports our physiological, metabolomic and biophysical evidence for G3P as the activator of ChREBP.

The G3P–ChREBP activation system suggests new mechanistic components of the Randle cycle and cooperation between ChREBP and other transcription factors

Philip Randle's medical school lectures, published in 1963, contained two simple sketches that depicted what he termed the glucose fatty-acid cycle[69]. The first sketch schematized glucose as the source of G3P, which is the backbone for triglyceride synthesis through the Kennedy pathway[70]. The second sketch illustrated Randle's observation that, in conditions of high fatty acid availability, there are mechanisms to block glycolysis and that, in conditions of high glucose availability, there are mechanisms to block fatty acid oxidation. In subsequent years, citrate production and inhibition of phosphofructokinase 1 were identified as mechanisms for fatty acid oxidation blocking glycolysis[71]. Regulation in what is termed the sweet side of the Randle cycle has been explained by the function of malonyl-coA as an essential substrate of fatty acid synthase and as an inhibitor of carnitine palmitoyltransferase 1, which mediates long-chain fatty acid (LCFA) entry into mitochondria[72]. Thus, when acetyl coA carboxylase converts cytosolic Ac-coA to malonyl-coA, it is committing carbon flow not only to synthesize LCFA but also to block LCFA oxidation.

Although Randle's principles of fuel utilization have been important in guiding research and medicine, many problems in metabolism remain elusive. For example, though fructose is known to be more lipogenic than glucose, it is not clear that this is fully explained on the basis of the higher affinity of fructokinase for fructose versus glucokinase for glucose, and the bypass of phosphofructokinase regulation[73]. According to our model, ChREBP evolved specifically to respond to the formation of G3P by stimulating transcription of enzymes that convert carbohydrates to LCFAs and transcription of Kennedy pathway enzymes that link LCFAs to G3P in triglyceride synthesis. Fructose would thus be more lipogenic than glucose because it results in greater ChREBP activation[59] because fructolysis (Fig. 1c) would tend to produce more G3P than glycolysis. Notably, because G3P is not a direct glycolytic intermediate such as DHAP or GA3P but rather an electron carrier in the GPDS, the production of G3P from carbohydrates is a signal of carbohydrate overload from diet, diabetes, *GCKR* variants or a signal that would be generated at normoglycaemia by fructose, ethanol, anoxia or mitochondrial insufficiency. Reductive stress was previously noted as a shared mechanism underlying metabolic features of both alcoholic and non-alcoholic hepatic steatosis via ChREBP activation[60]. Identification of G3P as the activator of ChREBP further unites the mechanisms of hepatic steatogenesis downstream of ethanol, fructose, hyperglycaemia and mitochondrial insufficiency.

We do not suggest that G3P-driven ChREBP-activated transcription is fully responsible for complex metabolic switches. Lipogenesis requires the activation of both ChREBP and SREBP-1c[62], which occurs with depression of the carnitine palmitoyltransferase and beta oxidation systems. By contrast, fasting-induced lipolysis, which is expected to produce G3P and activate ChREBP, also activates PPARα and the beta oxidation programme[27–29]. It is thus to be expected that complex interactions between fatty acid ligands, PPAR isoforms, SREBP and other transcription factors modulate the metabolic outputs of ChREBP in changing conditions. Two expected differences between G3P formation from glucose, ethanol and mitochondrial insufficiency (Fig. 1b) and G3P formation from lipolysis is that lipolytic G3P formation is expected to require GK activity and to produce PPARα-activating fatty acids (Fig. 1d). Thus, it is interesting to note that GK expression has been shown to drive lipolytic gene expression in the mouse liver, though this was attributed to the transcriptional activation of SREBP-1c rather than enzymatic activity[74].

The mouse CD model shows an ISR that may exacerbate urea cycle dysfunction

The integrated stress response (ISR) is an adaptive response to amino acid deprivation that is mediated by phosphorylation of eukaryotic translational initiation factor eIF2α, the production of specific transcription factors ATF4 and/or ATF5 and the resulting gene expression to restore protein homoeostasis[75]. Under conditions of protein limitation, new protein synthesis is focused on resolving amino acid deficiency. For example, FGF21 is an ISR-activated hormone that drives protein ingestion[76], whereas SLC3A2 is an ISR-activated transporter that increases cellular amino acid import[77]. The classical ISR-transcribed enzymes asparagine (Asn) synthetase (ASNS)[78] and cystathionine γ-lyase (CTH)[79] are induced to produce Asn and cysteine (Cys), respectively.

Mitochondrial defects are known to induce the ISR[80] via mechanisms that are not completely understood. However, it was shown that complex I inhibition of C2C12 mouse myoblasts induces the ISR

https://doi.org/10.1038/s42255-025-01399-3

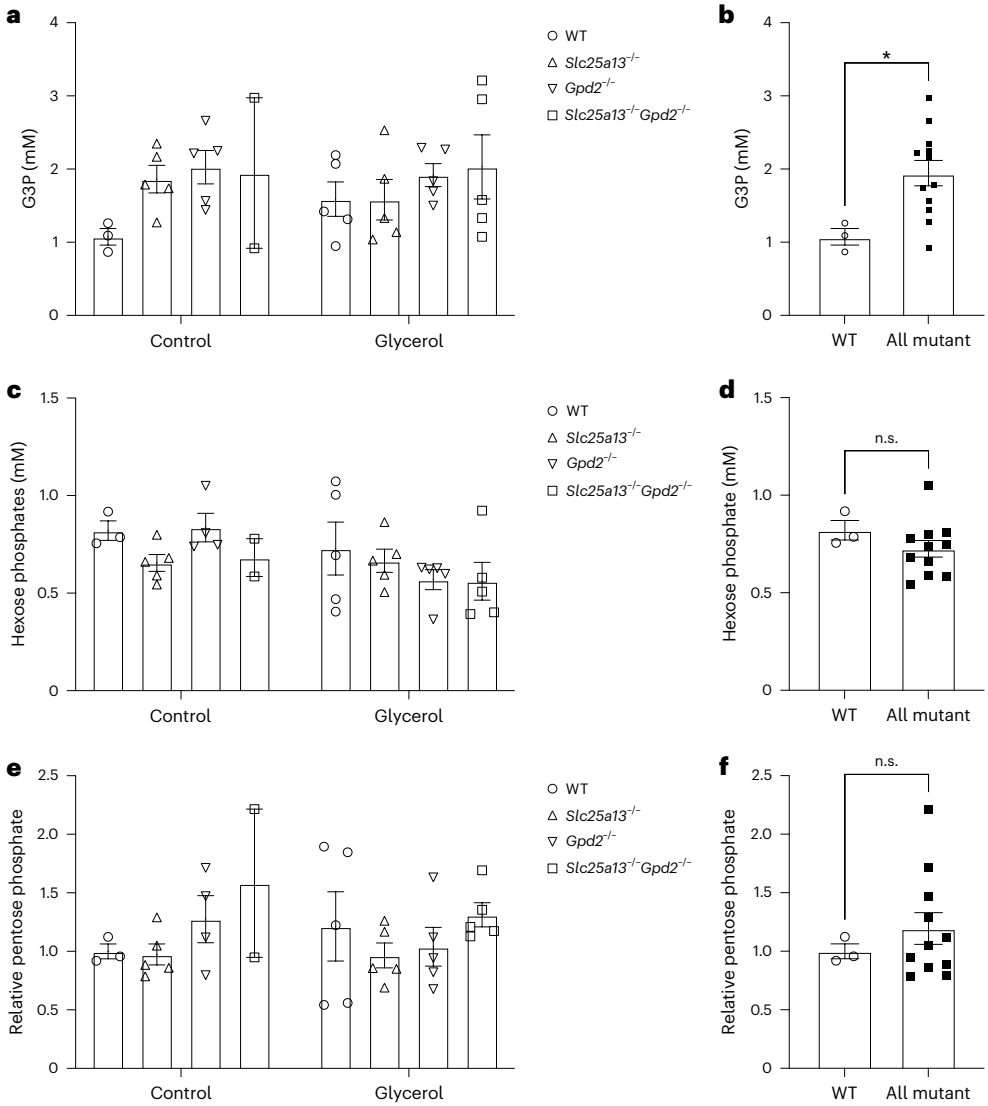

Fig. 4 | NADH shuttle disruption elevates hepatic G3P. a–**f**, We performed quantitative metabolomics for hepatic G3P (**a** and **b**) and hexose phosphates (**c** and **d**) and qualitative metabolomics for hepatic levels of pentose phosphates (**e** and **f**). The numbers of mice analysed were wild type (represented by circles, $n = 3$), *Slc25a13*$^{-/-}$ (represented by up triangles, $n = 5$), *Gpd2* (represented by down triangles, $n = 5$) and *Slc25a13*$^{-/-}$*Gpd2*$^{-/-}$ (represented by squares, $n = 2$) in mice with 2 days of ad libitim access to food and water. The numbers of mice analysed were wild type (represented by circles, $n = 5$), *Slc25a13*$^{-/-}$ (represented by triangles, $n = 5$), *Gpd2* (represented by down triangles, $n = 5$) and *Slc25a13*$^{-/-}$*Gpd2*$^{-/-}$ (represented by squares, $n = 5$) with 2 days of ad libitim access to food and 5% w/v glycerol. In **a**, **c** and **f**, all mouse genotypes were analysed separately. In **b**, **d** and **f**, the three mutant genotypes were pooled to compare wild type (represented by circles, $n = 3$) with the three genotypes containing one or both NADH shuttle systems disrupted (represented by filled squares, $n = 12$) with exposure to water. In **a**, the data show that each mutant genotype tends to have higher G3P than wild type and that glycerol tends to elevate G3P with respect to water. In **b**, the data show that the deletion of one or both NADH shuttle systems significantly elevates G3P ($P = 0.03$ by unpaired t-test, $t = 2.43$, degrees of freedom: 13). In **c** and **d**, no differences were observed in the hexose phosphate levels across the four genotypes and two conditions. In **e** and **f**, no differences were observed in the hexose phosphate levels across the four genotypes and two conditions. *$P < 0.05$. The error bars represent means ± s.e.m. n.s., not significant; WT, wild type.

by virtue of depressing Asp and Asn synthesis[81]. When amino acids are in limited supply, uncharged transfer RNAs (tRNAs) activate GCN2 protein kinase to phosphorylate eIF2α[82]. In myoblasts, the complex I inhibition-mediated induction of the ISR can be relieved by lowering the NADH/NAD$^+$ ratio and by provision of Asp or Ans[81].

RNA-seq data from the mouse model of CD supports Asp limitation as a mechanism by which the ISR can be activated by mitochondrial dysfunction in the liver. Further, the data suggest that the ISR may aggravate urea cycle dysfunction in CD. As shown in Fig. 6a, we noted that *Asns*[78] is strongly upregulated with deletion of *Slc25a13*. Moreover, with the inactivation of both NADH shuttle systems (Fig. 6b), additional components of an ISR were observed including elevation of the *Atf5* transcription factor[83]. Exposure of *Slc25a13*$^{-/-}$*Gpd2*$^{-/-}$ mice to glycerol (Fig. 6c) increased expression of *Slc3a2*[77] and *Cth*[79], which are recognized as part of the ISR[84].

As depicted in Fig. 6d, Asp is produced in mitochondria in a process requiring the activities of MDH2, GOT2 and the mitochondrial electron transfer chain[85]. Asp enters the cytosol through SLC25A13, where Asp is used for protein synthesis, ASNS-dependent conversion to Asn and nitrogen disposal through the urea cycle. As in the case of myoblasts treated with piericidin to inhibit complex I, which produced an ISR that was reversed by the provision of Asp or Asn[81], our data show that the loss of SLC25A13 is sufficient to induce an ISR. However, whereas the ISR evolved to be an adaptive system to resupply amino acids and restore protein homoeostasis[75], it is potentially maladaptive with respect to the ammonia disposal problem in CD because FGF21 may cause

https://doi.org/10.1038/s42255-025-01399-3

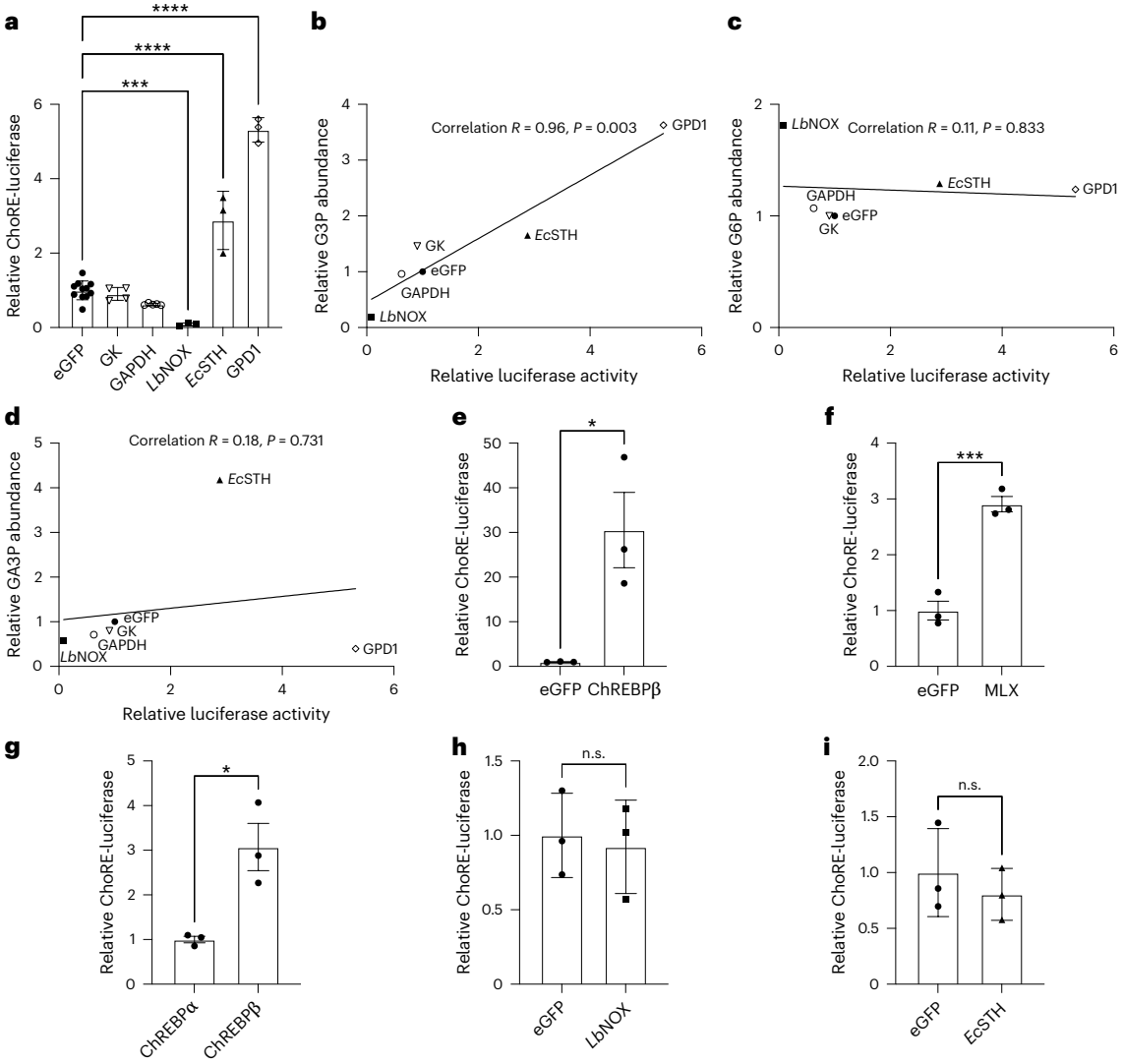

Fig. 5 | The ChREBPα-specific isoform of ChREBP is activated in a manner that is coincident with G3P accumulation. a, HEK293T cells cotransfected with ChREBPα, MLX, ChoRE-luciferase and the indicated genetic constructs were assessed for ChoRE-luciferase activity. The data show that *Lb*NOX depresses, *Ec*STH increases and GPD1 greatly increases ChoRE-luciferase activity. Significant differences between were calculated by applying one-way analysis of variance and Dunnett's multiple comparisons test in which ***$P < 0.0005$ and ****$P < 0.0001$. Numbers of biological replicates were: eGFP ($n = 11$); GK ($n = 4$); GPD1 ($n = 3$); GAPDH ($n = 5$); *Lb*NOX ($n = 3$); and *Ec*STH ($n = 3$). **b**–**d**, Relative levels of 137 metabolites were determined by LC–MS; by plotting ChoRE-luciferase activity against each metabolite, we show that G3P is highly correlated (CC of 0.96) with ChREBPα-dependent ChoRE-luciferase activity (**b**), whereas G6P (**c**) and GA3P (**d**) are not. *P* values tested the hypothesis of a non-zero slope. **e**, HEK293T cells cotransfected with ChREBPβ or eGFP plus ChoRE-luciferase were assessed for ChoRE-luciferase activity. Numbers of biological replicates were: eGFP ($n = 3$); ChREBPβ ($n = 3$); unpaired *t*-test (two-tailed), $P = 0.0248$. **f**, The HEK293T cells cotransfected with ChREBPβ with MLX or eGFP plus ChoRE-luciferase were assessed for ChoRE-luciferase activity. The numbers of biological replicates were: eGFP ($n = 3$); MLX ($n = 3$); unpaired *t*-test (two-tailed), $P = 0.0009$. **g**, HEK293T cells cotransfected with MLX plus ChoRE-luciferase plus either ChREBPα or ChREBPβ were assessed for ChoRE-luciferase activity. Numbers of biological replicates were: ChREBPα ($n = 3$): ChREBP β ($n = 3$); unpaired *t*-test (two-tailed), $P = 0.0178$. **h**,**i**, Finally, HEK293T cells cotransfected with ChREBPβ, MLX and ChoRE-luciferase plus were assayed for ChoRE-luciferase activity with either eGFP or *Lb*NOX (**h**) or *Ec*STH (**i**). There were three biological replicates for each sample. For **h**, the unpaired *t*-test (two-tailed): $P = 0.7680$. For **i**, the unpaired *t*-test (two-tailed): $P = 0.5023$. The data in **e** and **i** show that ChREBPβ has significant ChoRE-luciferase activity in HEK293T cells, **e**, that is, further boosted by MLX transfection, **f**. **g**, The data show that the ChoRE-luciferase activity of ChREBPβ-MLX exceeds that of ChREBPα-MLX. However, in contrast to the ability of *Lb*NOX to depress and *Ec*STH to increase ChoRE-luciferase activity of ChREBPα-MLX, **a**, ChREBPβ-MLX was not regulated by either *Lb*NOX, **h**, or *Ec*STH, **i**, thereby mapping the modulation of ChREBPα to the N-terminal GSM domain. Significant differences were calculated with unpaired *t*-tests in which *$P < 0.05$ and ***$P < 0.0005$. The error bars represent means ± s.e.m. n.s., not significant.

people to eat more protein[76], SLC3A2 will drive cellular amino acid import into hepatocytes already challenged by ammonia disposal[77], ASNS expression would tend to commit urea-cycle-limiting levels of Asp for Asn synthesis[78], and CTH enzyme activity directly produces ammonia[79]. Thus, we suggest that the partial inhibition of ATF5 and/or target enzymes such as ASNS and CTH could be considered as pharmacological approaches to improve urea cycle function in CD.

SLC25A13-mutation carriers have distinct metabolic traits and signs of potential FGF21 overexpression

Given the links between the loss of both copies of *SLC25A13* with liver disease and dietary preference in humans, we considered whether heterozygosity for *SLC25A13* disease mutations might be associated with anthropometrics, dietary patterns or unusual biomarkers. We used gnomAD[86] to assemble a list of the most commonly occurring

https://doi.org/10.1038/s42255-025-01399-3

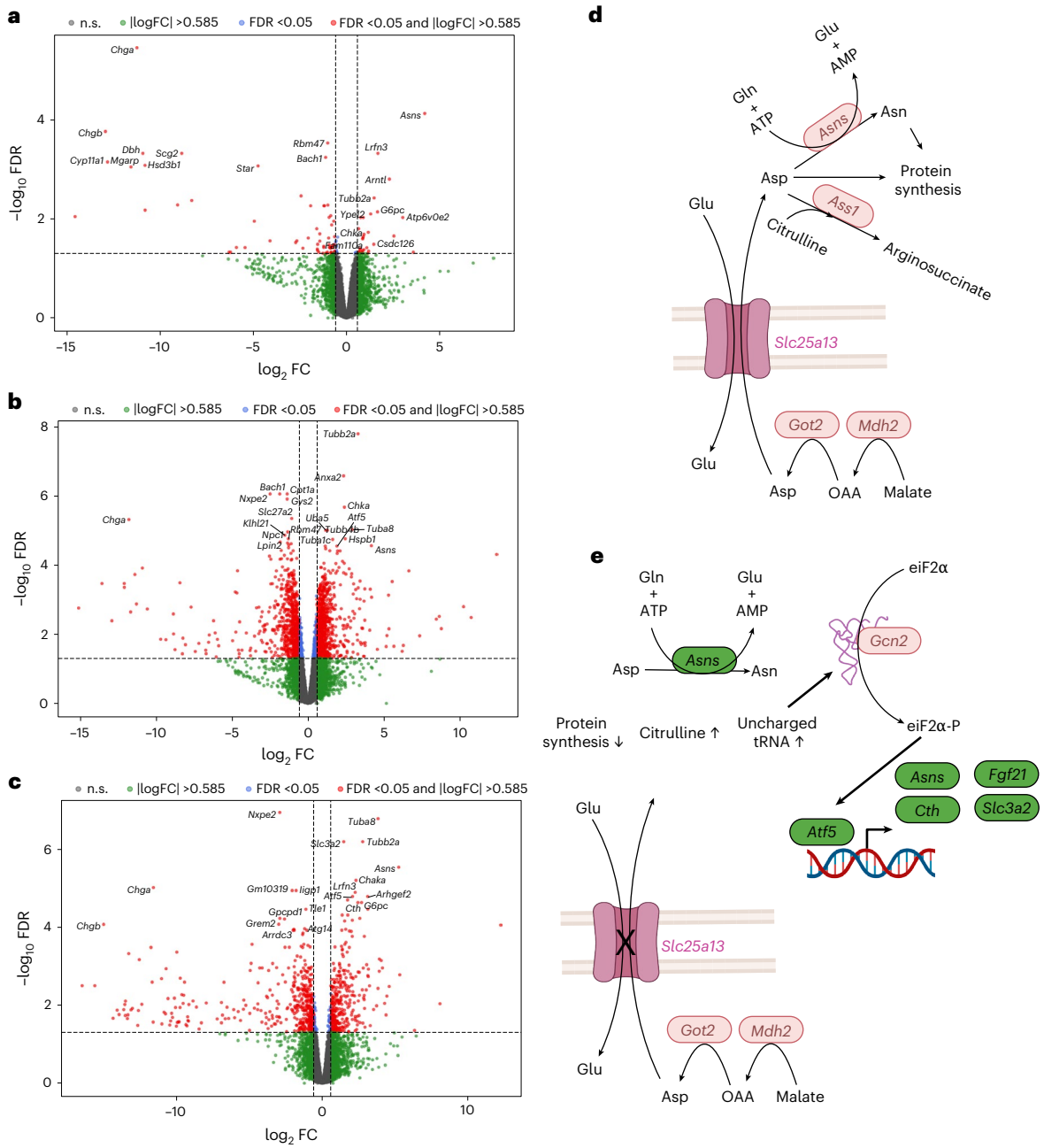

Fig. 6 | The murine CD model shows evidence of an ISR that may underly and aggravate urea cycle dysfunction. a–**c**, Differentially expressed hepatic genes shown in volcano plots for *slc25a13*$^{-/-}$ mice versus wild type (**a**), *slc25a13*$^{-/-}$*gpd2*$^{-/-}$ mice versus wild type (**b**) and *slc25a13*$^{-/-}$*gpd2*$^{-/-}$ glycerol-exposed mice versus wild-type water-exposed (**c**). **d**, Mitochondrial generation of Asp and the role of Slc25a13 in providing Asp to hepatocyte cytosol are depicted. Asp is consumed by Asn synthetase (Asns) to make Asn, is used in protein synthesis and is ligated to citrulline by argininosuccinate synthetase 1 (Ass1) in the urea cycle. **e**, An ISR is proposed to be initiated by shortage of cytosolic Asp and the consequent accumulation of uncharged tRNA Asp and/or tRNA Asn, which activate Gcn2 kinase activity on eIF2α. Subsequent induction of Atf5 and Atf5 target genes could aggravate the urea cycle dysfunction because Fgf21 drives protein ingestion, Slc3a2 increases amino acid uptake, Asns consumes Asp, further limiting the availability of Asp for nitrogen disposal, and Cth produces ammonia which may exacerbate the nitrogen disposal problem. FC, fold change; n.s., not significant; OAA, oxaloacetic acid. Panels **d** and **e** created with BioRender.com.

SLC25A13 alterations that are scored as pathological or likely pathological (Extended Data Table 2) and subjected them to several tests of genetic association. In deep phenotype genome-wide association studies, rs80338722 was moderately associated with body weight and body mass index in BioBank Japan ($P = 8.3 \times 10^{-6}$ and $P = 4.1 \times 10^{-4}$, respectively)[87] and associated with triglyceride levels in non-diabetic individuals[88], among other traits. Three additional alterations of *SLC25A13* variants were associated with total cholesterol[88], leptin[88] and autoimmune hepatitis[87]. Our interpretation of these data is that, at a population level, *SLC25A13* heterozygosity may bias the liver metabolism to produce greater G3P–ChREBP-dependent transcriptional output, which could either predispose to lipogenesis and/or produce a signal for elevated FGF21 as reported[89] for the *GCKR* polymorphism[44,46]. Indeed, based on known biology[90] and Mendelian randomization[91], one might expect higher FGF21 to be associated with higher sodium clearance from the kidney and with dietary preference for fatty fish versus sweets[76]. As shown in Fig. 7a, a phenome-wide association study for rs80338722 within BioBank Japan showed an association with low body weight. When we aggregated rare variant gene-based burden tests between *SLC25A13* alterations and

189 complex traits from the Common Metabolic Disease Knowledge Portal, the data suggested a distinct metabolic profile associated with low C-peptide and low incidence of type 1 diabetes but elevated levels of bilirubin and apolipoprotein B and a strong signal for high urinary sodium excretion (Fig. 7b). Consistent with the hypothesis that the inactivation of one copy of the *SLC25A13* gene elevates FGF21, common variant gene-based tests for *SLC25A13* and 189 complex traits from the Common Metabolic Disease Knowledge Portal[88] identified a strong association with oily fish consumption (Fig. 7c). This result is complementary to reports that a loss-of-function variant in *FGF21* is associated with higher sugar and alcohol consumption[92] and less desire for fish[93].

Data on human variation suggest that pathological *SLC25A13* mutations appeared multiple times in the Far East[15]. Our data suggest that loss-of-function allele persistence may be mediated by beneficial effects of FGF21 expression on renal function, insulin sensitivity and food choices. Indeed, if it is true that *SLC25A13*-mutation carriers circulate higher levels of FGF21, one might expect that lower ethanol and/or fructose consumption would protect their livers from the potentially lipogenic combination of these energy inputs with diminished flux through the MAS. Specifically, one might predict that *SLC25A13*-mutation carriers drink less alcohol than the general population but that those mutation carriers who drink have a greater hazard of hepatic steatosis.

Discussion

Just as rare mutations in model organisms have revealed the complexities of morphogenesis and gene regulation, many fundamental biological insights have been revealed from rare human diseases. In the case of CD, it became apparent that without a key component of the MAS, people and mice are sensitive to the development of MASLD despite being lean and do not enjoy sweets despite an intact initial preference for sweets. We propose that a key to both of these CD presentations is the accumulation of hepatic G3P. The G3P-ChREBP programme drives a lipogenic transcriptional programme that induces *Pklr*, *Acly*, *Acaca*, *Fasn*, *Elovl6* and other genes to synthesize LCFAs and *Agpat2* and other genes to link newly synthesized LCFAs to the G3P backbone for triglyceride synthesis. Notably, the product of *Acaca*, malonyl-coA, is not only the key substrate for LCFA synthesis but also the key inhibitor of LCFA entry into mitochondria for β-oxidation[72]. Thus, G3P activation of ChREBP has the potential to transcriptionally direct triglyceride synthesis causing hepatic steatogenesis while also promoting resistance to hepatic lipolysis. Indeed, based on the low ATP state of the liver in CD models[21], one might have expected brisk usage of stored hepatic triglycerides during the fasting daytime of CD mice or the fasting nighttime of patients with CD. However, the fact that lean MASLD is common in CD[18] and the clinical observation that MCTs are preferable to common fats[5] suggest that CPT1A may be inhibited in CD, thereby rendering stored triglycerides to be resistant to oxidation. In addition, at the RNA level, our data show that the *Slc25a13*$^{-/-}$*Gpd2*$^{-/-}$ model significantly depresses expression of *Cpt1a* (Fig. 6b). Thus, patients with CD and others with MASLD driven by the proposed G3P–ChREBP lipogenesis programme may benefit from small molecule activators of CPT1A[94]. Additionally, it may be worth testing activators of AMP kinase[95], which would be expected to turn off Ac-coA carboxylase and thereby relieve CPT1A inhibition.

It is notable that the FGF21 induction system responds to a number of conditions of metabolic stress including fasting and the ingestion of fructose and ethanol. Although FGF21 signals to the brain to limit sweets and alcohol and to eat protein[76], it also makes complex signals to the periphery, which have the potential to treat common MASLD[96]. Discovery of the G3P–ChREBP induction system suggests strategies to develop lipidated prodrugs of G3P that would induce FGF21 expression, potentially in combination with fibrates to activate PPARα-dependent lipolysis and synergistically superinduce FGF21[27,29]. Although chronic FGF21-elevated conditions such as mitochondrial disease are potentially FGF21-resistant[43], G3P-releasing FGF21-inducing prodrugs that increase energy expenditure and alter food choices could be valuable to address overweight and MASLD, particularly if combined with glucagon-like peptide-1 receptor agonists[97].

Though ChREBP has long been known to connect carbohydrate oxidation to lipogenesis[48–50], and G3P has long been known to serve as the backbone for triglyceride synthesis[70] with a unique location in the glucose fatty-acid cycle[69], the accumulation of G3P and induction of a G3P–ChREBP transcriptional programme in the mouse model of CD allowed us to propose that the most distinctive presentations of CD, namely sweet aversion, lean MASLD and the beneficial effects of MCTs in CD are due to G3P–ChREBP signalling. Ongoing work will further probe the components of FGF21 transcriptional induction mechanisms and determine how the ISR and ChREBP induction systems interact in health and disease.

Methods

Generation of mice and mouse samples

All mouse breeding and experiments were performed with protocols approved by the City of Hope Institutional Animal Care and Use Committee and Institutional Biosafety Committee. Sperm from a male *Slc25a13*$^{-/-}$*Gpd2*$^{-/-}$ C57BL6/J mouse[14] were a kind gift of Dr Saheki and the Citrin Foundation. In vitro fertilization was performed with C57BL6/J eggs and a pseudopregnant C57BL6/J female recipient by Walter Tsark in the City of Hope Transgenic Mouse Core. The resulting diheterozygous offspring were intercrossed to generate wild-type, *Slc25a13*$^{-/-}$, *Gpd2*$^{-/-}$ and *Slc25a13*$^{-/-}$*Gpd2*$^{-/-}$ mice of both sexes. At weaning, genotypes were determined by the polymerase chain reaction of tail tissues (Transnetyx), and mice were single-sex group-housed until experimental use. The mice were maintained at 21 °C under a standard 12–12-h light–dark cycle and provided with ad libitim access to food and water. For analysis of FGF21 expression, hepatic gene expression and metabolite accumulation, 8 to 16-week-old mice were single-housed with chow (LabDiet irradiated PicoLab Rodent Diet 20, 5053) and a single bottle of either water or 5% (w/v) glycerol for 2 days. Mice were then killed by decapitation via guillotine without sedation and exsanguinated with a funnel for blood collection into 1.5-ml microcentrifuge tubes on ice, and livers were freeze-clamped in liquid nitrogen immediately after collection[98,99]. Sera were obtained by centrifuging blood at 8,000*g* for 10 min at 4 °C. Liver samples were pulverized with a mortar and pestle cooled by liquid nitrogen. Data for all mouse samples are provided in Source Data Figs. 2–4.

Fig. 7 | Locus-wide and gene-based association plots for *SLC25A13*. **a**, Phenome-wide association study for rs80338722 within BioBank Japan identified an association with low body weight. The *x* axis represents phenotypes within Biobank Japan, whereas the *y* axis is the $-\log_{10}(P\text{ value})$ for the association between rs80338722 and each trait. The dashed grey line represents the moderate significance threshold ($P < 1 \times 10^{-3}$). **b**, The aggregated rare variant gene-based burden tests between *SLC25A13* and 189 complex traits from the Common Metabolic Disease Knowledge Portal identified phenotypic associations, including high urinary sodium excretion and elevated bilirubin. The traits above the orange dashed line (significance threshold $P < 5 \times 10^{-2}$) are statistically significant. Tiangles pointing up indicate associations with increased trait levels or disease risk, whereas the triangles pointing down indicate associations with decreased traits levels or disease risk. **c**, Common variant gene-based tests for *SLC25A13* and 189 complex traits from the Common Metabolic Disease Knowledge Portal identified a strong association with oily fish consumption. Traits above the orange dashed line (threshold $P < 2.5 \times 10^{-6}$) are nominally significant. ApoA, apolipoprotein A; ApoB, apolipoprotein B; BMI, body mass index; adj, adjusted; HDL, high density lipoprotein; ASCVD, atherosclerotic cardiovascular disease; NAFLD, nonalcoholic fatty liver disease; HOMA-IR, homeostatic model assessment of insulin resistance; CCS, coronary calcium score.

https://doi.org/10.1038/s42255-025-01399-3

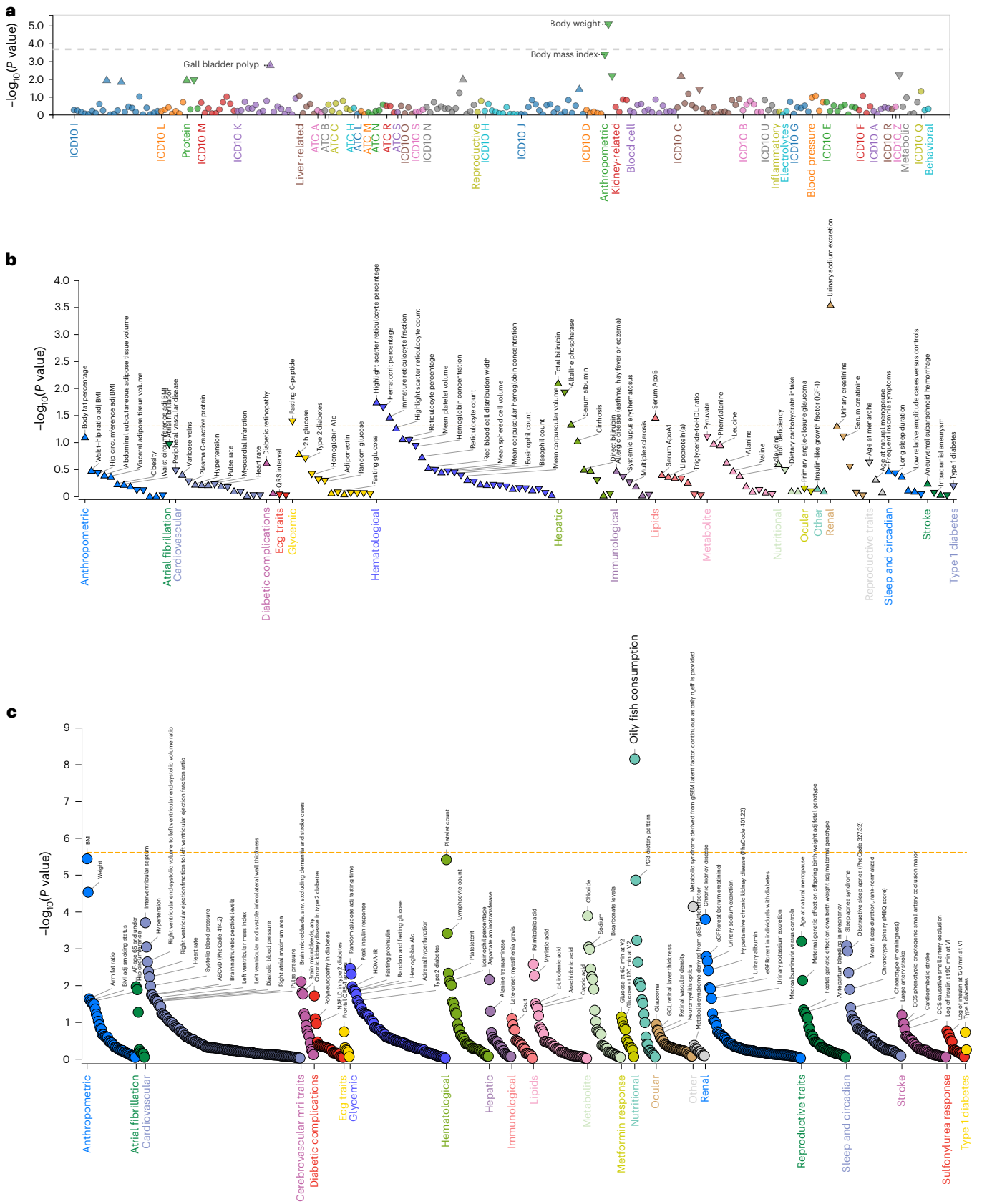

FGF21 quantification

The Mouse/Rat FGF21 Quantikine ELISA Kit from R&D Systems (MF2100) was used for FGF21 quantification of mouse sera. A total of 50 µl of assay diluent RD1-41 was added to each well followed by equal volumes of standard, control and experimental samples. After incubation for 2 h at room temperature, wells were aspirated and washed five times with 400 µl of wash buffer. A total of 100 µl of horseradish-peroxidase-conjugated FGF21 antibody solution was then added to each well and incubated at room temperature for 2 h followed by five washes with 400 µl of wash buffer. After washing, 100 µl of freshly prepared substrate was added to each well and incubated for 30 min at room temperature. Assays were terminated with the addition of 100 µl of stop solution followed by reading at 450 nm with wavelength correction at 570 nm.

RNA-seq

The 20-mg liver aliquots were used for RNA isolation (Qiagen, RNeasy Mini Kit, 74104) and DNase I treatment (Qiagen, RNase-Free DNase Set, 79254). RNA integrity was assessed using an Agilent 4200 Tapestation, ensuring an RNA integrity number >5.0 for all samples. Library preparation and sequencing was performed by 7 Traits Genomics. Libraries were prepared using the NEBNext UltraExpress RNA Library Prep Kit (New England Biolabs), following the manufacturer's protocol using 150 ng of RNA per sample. Messenger RNA (mRNA) was enriched using poly(A) selection. Enriched mRNA was fragmented, reverse-transcribed and converted to cDNA. The cDNA underwent end repair, adaptor ligation and size selection. Polymerase chain reaction amplification was performed (11 cycles) to ensure a sufficient library yield while minimizing amplification bias. Library quality and size distribution were assessed using a Tapestation and quantified by Qubit (Thermo Fisher Scientific). The libraries were pooled on an equimolar basis and sequenced on an Illumina NovaSeq X Plus platform using a 25B lane configuration with paired-end 150-bp reads with a minimum of 20 million paired reads per sample. Base calling and demultiplexing were performed using Illumina's DRAGEN Bio-IT platform. Raw sequencing reads were processed for quality control using FastQC and trimmed to remove adaptors and low-quality bases using Trimmomatic[100] and poly(A) tails using FASTP[101]. Processed reads were mapped back to the mouse genome (mm10) using STAR software (v. 2.6.0.a)[102]. HTSeq software (v.0.11.1) was used to generate the count matrix with default parameters[103]. Differential expression analysis was performed by normalizing read counts to expression values using the trimmed mean of M values normalization method in edgeR[104,105]. Generalized linear models were applied to identify differentially expressed genes between glycerol and water-exposed liver samples of the same genotype or between liver samples of different genotypes. Normalized expression levels from the trimmed mean of M values were used as the dependent variable, whereas sequencing batches were included as an independent variable to account for batch effects. Genes with a false-discovery-rate-adjusted *P*value below 0.05 and a fold change greater than 2 or less than 0.5 were classified as significantly upregulated or downregulated, respectively.

Metabolomic analysis of mouse livers

For G3P quantification, 2.0-mg samples of pulverized frozen liver were spiked with ^{13}C3-G3P (2.28 µM final concentration, Sigma-Aldrich). Frozen samples were rapidly processed with a boiling buffered ethanol extraction (600 µl of 25% 10 mM HEPES buffer and 75% ethanol) followed by vigorous vortexing. Samples were placed on a thermomixer for 5 min at 55 °C with shaking at 1,200 rpm then cooled on ice for 30 s. Samples were then placed in a water bath sonicator for 1 min followed by an additional 30 s on ice. Samples were clarified by centrifugation at 16,100*g* in a prechilled centrifuge at 4 °C; the supernatants were transferred to clean tubes followed by a second round of centrifugation. Clarified supernatants were transferred to new tubes and dried for 5 h in a vacuum centrifuge at 4 °C. Dried samples were resuspended in 80 µl of liquid chromatography–mass spectrometry (LC–MS) water. In total, 20-fold-diluted samples were transferred to mass spectrometry vials for analysis by liquid chromatography–tandem mass spectrometry. For the analysis of hexose phosphates and pentose phosphates, 2.0-mg samples of pulverized frozen liver were spiked with a ^{13}C glucose-grown yeast extract (ISO101, Cambridge Isotope Laboratories) as an internal standard[106], and the same workup was performed. The samples were analysed on a Vanquish Horizon UHPLC with a tandem Thermo Scientific Orbitrap Fusion mass spectrometer. The vials were maintained in autosampler at 4 °C. The instrument source parameters were held at 3 kV negative ion spray voltage, 300 °C ion transfer tube temperature, 250 °C vaporizer temperature, sheath gas of 20, auxiliary gas of 10 and sweep gas of 3. The liquid chromatography separation was carried out using an Acquity Premier HSS T3 column with VanGuard FIT, 1.8 µm, 2.1 mm × 150 mm with mobile phases A (5 mM tributylamine and 10 mM acetic acid with 5% v/v methanol in LC–MS-grade water) and B (LC–MS-grade methanol) at a constant flow rate of 0.5 ml min^{-1}. The separation was carried out with a starting condition of 0% B; 0–10 min, 10.5% B; 10–18 min, 52.6% B; 18–19 min, 52.6% B; 19–20 min, 0% B; and 20–26 min, 0% B. Spectra for G3P were acquired using a targeted MS2 scan with parent ion of *m*/*z* 171.0058 with collision energy 25. Spectra for ^{13}C3-G3P were acquired with parent ion *m*/*z* of 174.0165 with collision energy 25 with the primary fragment ion of *m*/*z* 78.9588. The hexose phosphate spectra were acquired using a targeted MS2 scan of parent ion *m*/*z* 259.0198. The ^{13}C6-hexose phosphate spectra were acquired with a parent ion of *m*/*z* 265.0426 with collision energy of 20 and primary fragment ion *m*/*z*96.9690. The hexose phosphate spectra signals were predominantly from G6P, fructose-6-phosphate and glucose-1-phosphate, determined with pure synthetic standards. The pentose phosphate spectra were acquired using the targeted MS2 scan for the parent ion *m*/*z* 229.0124 at collision energy 30 with a primary fragment ion *m*/*z* of 78.9588. The pentose phosphate spectra were predominantly composed of ribose-5-phosphate, ribose-1-phosphate and X5P. The mass spectra data were analysed using the open source-software, Skyline v25.1.

Cellular reconstitution of ChREBP-MLX-dependent ChORE-luciferase activity

Human ChREBPα (accession number NM_032951.3), human ChREBPβ (accession number XM_047420437.1), human MLX (accession number NM_170607.3) and eGFP coding sequences were synthesized by Genewiz and cloned into pcDNA3.1 vectors (Invitrogen). GK was subcloned into pcDNA3.1 (Invitrogen) from pWZL-Neo-Myr-Flag-GK (Addgene plasmid 20493). pcDNA3.1-GPD1 and pcDNA3.1-GAPDH were purchased from GenScript (clone ID: OHu20325 and OHu20566). Plasmids pcDNA3.1-*Lb*NOX, pcDNA3.1-*Ec*STH, pGL4.14 [luc2/Hygro]-ChoRE and pGL4.75[hRluc/CMV] were as described[60]. HEK293T cells (ATCC catalogue CRL-3216) were seeded into 24-well plates and maintained in Dulbecco's modified Eagle medium (Gibco) with 10% foetal bovine serum (Gibco) and 1% Pen-Strep (Gibco) at 37 °C and 5% CO_2 overnight. On the following day, media were replaced by OPTI-MEM (Gibco) 1 h before plasmid cotransfection. Lipofectamine 3000 reagent (Invitrogen) was used for cotransfections for 5 h, after which media were replaced with Dulbecco's modified Eagle medium containing 10% foetal bovine serum for 48 h. The cells were then collected, and luciferase assays were performed using the Firefly and Renilla Single Tube Luciferase Assay Kit (Biotium) following the manufacturer's protocol. A Tecan Infinite M Plex plate reader was used to measure Firefly and *Renilla* luminescence. Firefly luciferase values were normalized to corresponding *Renilla*luciferase measurements to correct for cell quantity and transfection efficiency. The underlying data are provided in Source Data Fig. 5.

Metabolomic analysis of transfected HEK293T cells

HEK293T cells were seeded into six-well plates overnight and then underwent plasmid cotransfection as described above for 48 h. Cells were then washed with phosphate-buffered saline, quenched with dry ice-cold 80% methanol and transferred to conical tubes. Relative quantification of 137 metabolites was performed as described[60].

Biophysical characterization of the ChREBP GSM

The coding sequence for mouse ChREBPα (amino acids 43 to 307) was converted to *E. coli*-optimized codons and inserted into a pET vector carboxyl to $MetHis_6$. The plasmid, pVB240306, was transformed into in *E. coli* Arctic Express, and expression was induced at 12.5 °C with 1 mM IPTG for 18 h. Total protein from the 1-litre culture was solubilized in 15 ml of denaturing lysis buffer (8 M urea, 100 mM NaH_2PO_4, 10 mM Tris Cl, pH 8.0, 0.05% Tween 20). The recombinant protein was captured by overnight incubation with 3 ml of Ni-NTA resin (Qiagen) followed by washing with 30 ml of denaturing buffer (8 M urea, 100 mM NaH_2PO_4, 10 mM Tris Cl, pH 6.3, 0.05% Tween 20). On-column protein refolding was performed by washing with 30 ml of 50 mM NaH_2PO_4, pH 8.0, 300 mM NaCl, 0.1% Triton X-100, followed by 30 ml of 50 mM NaH_2PO_4, pH 8.0, 300 mM NaCl, 5 mM β-cyclodextrin, 0.05% Tween 20 and 30 ml of 50 mM NaH_2PO_4, pH 8.0, 500 mM NaCl, 0.05% Tween 20. His-tagged ChREBP43–307 was recovered in 50 mM NaH_2PO_4, pH 8.0, 300 mM NaCl, 0.05% Tween 20, 350 mM imidazole at a yield of 1–2 mg l^{-1} of culture. All ligands were prepared in the same buffer. Ligand binding was determined by isothermal titration calorimetry using a Nano ITC (TA Instruments) to measure ligand concentration-dependent heat changes. Ligands were delivered in a 50-µl syringe to 185 µl of His-tagged ChREBP43–307 in the sample cell. After an initial 0.8-µl injection, 19 additional 2.5-µl injections were made with a time interval of 200 s between each injection. Measurements were made at 20 °C with stirring at 250 rpm. Informative ligand concentrations were determined empirically to observe saturable binding. Binding profiles were fitted to a blank and independent model with single-site binding using analysis software supplied with the instrument. Each experiment was performed in triplicate.

Statistics and reproducibility

Because the effect sizes and the variability of gene expression, FGF21 expression and metabolite levels were unknown until these experiments were performed, it was not possible to predetermine animal sample sizes. The size of mouse groups was limited by the availability of male and female *Slc25a13*$^{-/-}$*Gpd2*$^{-/-}$ mice, which were obtained at lower than Mendelian ratios. Mice of each of the four genotypes were randomly assigned to water or glycerol exposure. Sera and frozen liver powders were stored in numbered tubes and were analysed by investigators who were blinded to genotype and treatment. Sera that were haemolysed were excluded from FGF21 quantification. Data distributions were assumed to be normal, but this was not formally tested. Statistical analysis was performed with GraphPad Prism software. Details of the statistical tests and the numbers of replicates are provided in the figure legends.

Reporting summary

Further information on research design is available in the Nature Portfolio Reporting Summary linked to this article.

Data availability

The mouse data, protein purification data and isothermal titration calorimetry data are available via OSF at https://osf.io/j5veb. The RNA-seq data are available via the Gene Expression Omnibus with accession no. GSE304958. The metabolomic data for Figs. 4 and 5 are available via the Metabolomics Workbench with accession nos. ST004126 and ST004125, respectively. The plasmids are available via Addgene. Source data are provided with this paper.

References

1. Palmieri, L. et al. Citrin and aralar1 are Ca^{2+}-stimulated aspartate/glutamate transporters in mitochondria. *EMBO J.* **20**, 5060–5069 (2001).
2. Saheki, T. & Kobayashi, K. Mitochondrial aspartate glutamate carrier (citrin) deficiency as the cause of adult-onset type II citrullinemia (CTLN2) and idiopathic neonatal hepatitis (NICCD). *J. Hum. Genet.* **47**, 333–341 (2002).
3. Saheki, T. et al. Metabolic derangements in deficiency of citrin, a liver-type mitochondrial aspartate-glutamate carrier. *Hepatol. Res.* **33**, 181–184 (2005).
4. Grunert, S. C. et al. Citrin deficiency mimicking mitochondrial depletion syndrome. *BMC Pediatr.* **20**, 518 (2020).
5. Saheki, T., Moriyama, M., Funahashi, A. & Kuroda, E. AGC2 (citrin) deficiency—from recognition of the disease till construction of therapeutic procedures. *Biomolecules* https://doi.org/10.3390/biom10081100 (2020).
6. Lin, Y. et al. Combining newborn metabolic and genetic screening for neonatal intrahepatic cholestasis caused by citrin deficiency. *J. Inherit. Metab. Dis.* **43**, 467–477 (2020).
7. Kikuchi, A. et al. Simple and rapid genetic testing for citrin deficiency by screening 11 prevalent mutations in SLC25A13. *Mol. Genet. Metab.* **105**, 553–558 (2012).
8. Kido, J., Makris, G., Santra, S. & Haberle, J. Clinical landscape of citrin deficiency: a global perspective on a multifaceted condition. *J. Inherit. Metab. Dis.* **47**, 1144–1156 (2024).
9. Kim, S. Y. & Yi, D. Y. Components of human breast milk: from macronutrient to microbiome and microRNA. *Clin. Exp. Pediatr.* **63**, 301–309 (2020).
10. Belenky, P., Bogan, K. L. & Brenner, C. NAD^+ metabolism in health and disease. *Trends Biochem. Sci.* **32**, 12–19 (2007).
11. Bricker, D. K. et al. A mitochondrial pyruvate carrier required for pyruvate uptake in yeast, *Drosophila*, and humans. *Science* **337**, 96–100 (2012).
12. Goyal, S. et al. Dynamics of SLC25A51 reveal preference for oxidized NAD^+ and substrate led transport. *EMBO Rep.* **24**, e56596 (2023).
13. Dawson, A. G. Oxidation of cytosolic NADH formed during aerobic metabolism in mammalian cells. *Trends Biochem. Sci.* **4**, 171–176 (1979).
14. Saheki, T. et al. Citrin/mitochondrial glycerol-3-phosphate dehydrogenase double knock-out mice recapitulate features of human citrin deficiency. *J. Biol. Chem.* **282**, 25041–25052 (2007).
15. Tavoulari, S., Lacabanne, D., Thangaratnarajah, C. & Kunji, E. R. S. Pathogenic variants of the mitochondrial aspartate/glutamate carrier causing citrin deficiency. *Trends Endocrinol. Metab.* **33**, 539–553 (2022).
16. Gonzalez-Moreno, L. et al. Exogenous aralar/slc25a12 can replace citrin/slc25a13 as malate aspartate shuttle component in liver. *Mol. Genet. Metab. Rep.* **35**, 100967 (2023).
17. Saheki, T. et al. Reduced carbohydrate intake in citrin-deficient subjects. *J. Inherit. Metab. Dis.* **31**, 386–394 (2008).
18. Komatsu, M. et al. Citrin deficiency as a cause of chronic liver disorder mimicking non-alcoholic fatty liver disease. *J. Hepatol.* **49**, 810–820 (2008).
19. Fukushima, K. et al. Conventional diet therapy for hyperammonemia is risky in the treatment of hepatic encephalopathy associated with citrin deficiency. *Intern. Med.* **49**, 243–247 (2010).
20. Sinasac, D. S. et al. *Slc25a13*-knockout mice harbor metabolic deficits but fail to display hallmarks of adult-onset type II citrullinemia. *Mol. Cell. Biol.* **24**, 527–536 (2004).
21. Saheki, T. et al. Oral aversion to dietary sugar, ethanol and glycerol correlates with alterations in specific hepatic metabolites in a mouse model of human citrin deficiency. *Mol. Genet. Metab.* **120**, 306–316 (2017).

22. Flippo, K. H. & Potthoff, M. J. Metabolic messengers: FGF21. *Nat. Metab.* **3**, 309–317 (2021).
23. Jensen-Cody, S. O. et al. FGF21 signals to glutamatergic neurons in the ventromedial hypothalamus to suppress carbohydrate intake. *Cell Metab.* **32**, 273–286 e276 (2020).
24. Flippo, K. H. et al. FGF21 suppresses alcohol consumption through an amygdalo-striatal circuit. *Cell Metab.* **34**, 317–328 e316 (2022).
25. Xu, J. et al. Fibroblast growth factor 21 reverses hepatic steatosis, increases energy expenditure, and improves insulin sensitivity in diet-induced obese mice. *Diabetes* **58**, 250–259 (2009).
26. Zouhar, P. et al. A pyrexic effect of FGF21 independent of energy expenditure and UCP1. *Mol. Metab.* **53**, 101324 (2021).
27. Inagaki, T. et al. Endocrine regulation of the fasting response by PPARα-mediated induction of fibroblast growth factor 21. *Cell Metab.* **5**, 415–425 (2007).
28. Potthoff, M. J. et al. FGF21 induces PGC-1α and regulates carbohydrate and fatty acid metabolism during the adaptive starvation response. *Proc. Natl Acad. Sci. USA* **106**, 10853–10858 (2009).
29. Badman, M. K. et al. Hepatic fibroblast growth factor 21 is regulated by PPARα and is a key mediator of hepatic lipid metabolism in ketotic states. *Cell Metab.* **5**, 426–437 (2007).
30. Forman, B. M., Chen, J. & Evans, R. M. Hypolipidemic drugs, polyunsaturated fatty acids, and eicosanoids are ligands for peroxisome proliferator-activated receptors α and δ. *Proc. Natl Acad. Sci. USA* **94**, 4312–4317 (1997).
31. Uebanso, T. et al. Paradoxical regulation of human FGF21 by both fasting and feeding signals: is FGF21 a nutritional adaptation factor? *PLoS ONE* **6**, e22976 (2011).
32. Soberg, S. et al. FGF21 is a sugar-induced hormone associated with sweet intake and preference in humans. *Cell Metab.* **25**, 1045–1053 e1046 (2017).
33. von Holstein-Rathlou, S. et al. FGF21 mediates endocrine control of simple sugar intake and sweet taste preference by the liver. *Cell Metab.* **23**, 335–343 (2016).
34. Iroz, A. et al. A specific ChREBP and PPARα cross-talk is required for the glucose-mediated FGF21 response. *Cell Rep.* **21**, 403–416 (2017).
35. Dushay, J. R. et al. Fructose ingestion acutely stimulates circulating FGF21 levels in humans. *Mol. Metab.* **4**, 51–57 (2015).
36. Fisher, F. M. et al. A critical role for ChREBP-mediated FGF21 secretion in hepatic fructose metabolism. *Mol. Metab.* **6**, 14–21 (2017).
37. Galman, C. et al. The circulating metabolic regulator FGF21 is induced by prolonged fasting and PPARα activation in man. *Cell Metab.* **8**, 169–174 (2008).
38. Kim, K. H. et al. Acute exercise induces FGF21 expression in mice and in healthy humans. *PLoS ONE* **8**, e63517 (2013).
39. Cuevas-Ramos, D. et al. Exercise increases serum fibroblast growth factor 21 (FGF21) levels. *PLoS ONE* **7**, e38022 (2012).
40. Markan, K. R. et al. Circulating FGF21 is liver derived and enhances glucose uptake during refeeding and overfeeding. *Diabetes* **63**, 4057–4063 (2014).
41. Zhang, X. et al. Serum FGF21 levels are increased in obesity and are independently associated with the metabolic syndrome in humans. *Diabetes* **57**, 1246–1253 (2008).
42. Chen, W. W. et al. Circulating FGF-21 levels in normal subjects and in newly diagnose patients with type 2 diabetes mellitus. *Exp. Clin. Endocrinol. Diabetes* **116**, 65–68 (2008).
43. Tyynismaa, H. et al. Mitochondrial myopathy induces a starvation-like response. *Hum. Mol. Genet.* **19**, 3948–3958 (2010).
44. Cheung, C. Y. Y. et al. An exome-chip association analysis in Chinese subjects reveals a functional missense variant of GCKR that regulates FGF21 levels. *Diabetes* **66**, 1723–1728 (2017).
45. Desai, B. N. et al. Fibroblast growth factor 21 (FGF21) is robustly induced by ethanol and has a protective role in ethanol associated liver injury. *Mol. Metab.* **6**, 1395–1406 (2017).
46. Goodman, R. P. et al. Hepatic NADH reductive stress underlies common variation in metabolic traits. *Nature* **583**, 122–126 (2020).
47. Laeger, T. et al. FGF21 is an endocrine signal of protein restriction. *J. Clin. Invest.* **124**, 3913–3922 (2014).
48. Katz, L. S., Baumel-Alterzon, S., Scott, D. K. & Herman, M. A. Adaptive and maladaptive roles for ChREBP in the liver and pancreatic islets. *J. Biol. Chem.* **296**, 100623 (2021).
49. Abdul-Wahed, A., Guilmeau, S. & Postic, C. Sweet sixteenth for ChREBP: established roles and future goals. *Cell Metab.* **26**, 324–341 (2017).
50. Kawaguchi, T., Osatomi, K., Yamashita, H., Kabashima, T. & Uyeda, K. Mechanism for fatty acid "sparing" effect on glucose-induced transcription: regulation of carbohydrate-responsive element-binding protein by AMP-activated protein kinase. *J. Biol. Chem.* **277**, 3829–3835 (2002).
51. Ma, L., Robinson, L. N. & Towle, H. C. ChREBP•Mlx is the principal mediator of glucose-induced gene expression in the liver. *J. Biol. Chem.* **281**, 28721–28730 (2006).
52. Herman, M. A. et al. A novel ChREBP isoform in adipose tissue regulates systemic glucose metabolism. *Nature* **484**, 333–338 (2012).
53. Shih, H. M., Liu, Z. & Towle, H. C. Two CACGTG motifs with proper spacing dictate the carbohydrate regulation of hepatic gene transcription. *J. Biol. Chem.* **270**, 21991–21997 (1995).
54. Li, M. V., Chang, B., Imamura, M., Poungvarin, N. & Chan, L. Glucose-dependent transcriptional regulation by an evolutionarily conserved glucose-sensing module. *Diabetes* **55**, 1179–1189 (2006).
55. McFerrin, L. G. & Atchley, W. R. A novel N-terminal domain may dictate the glucose response of Mondo proteins. *PLoS ONE* **7**, e34803 (2012).
56. Li, M. V. et al. Glucose-6-phosphate mediates activation of the carbohydrate responsive binding protein (ChREBP). *Biochem. Biophys. Res. Commun.* **395**, 395–400 (2010).
57. Arden, C. et al. Fructose 2,6-bisphosphate is essential for glucose-regulated gene transcription of glucose-6-phosphatase and other ChREBP target genes in hepatocytes. *Biochem. J.* **443**, 111–123 (2012).
58. Kabashima, T., Kawaguchi, T., Wadzinski, B. E. & Uyeda, K. Xylulose 5-phosphate mediates glucose-induced lipogenesis by xylulose 5-phosphate-activated protein phosphatase in rat liver. *Proc. Natl Acad. Sci. USA* **100**, 5107–5112 (2003).
59. Kim, M. S. et al. ChREBP regulates fructose-induced glucose production independently of insulin signaling. *J. Clin. Invest.* **126**, 4372–4386 (2016).
60. Singh, C. et al. ChREBP is activated by reductive stress and mediates GCKR-associated metabolic traits. *Cell Metab.* **36**, 144–158 (2024).
61. Kukurba, K. R. & Montgomery, S. B. RNA sequencing and analysis. *Cold Spring Harb. Protoc.* **2015**, 951–969 (2015).
62. Linden, A. G. et al. Interplay between ChREBP and SREBP-1c coordinates postprandial glycolysis and lipogenesis in livers of mice. *J. Lipid Res.* **59**, 475–487 (2018).
63. Li, B. & Dewey, C. N. RSEM: accurate transcript quantification from RNA-Seq data with or without a reference genome. *BMC Bioinf.* **12**, 323 (2011).
64. Ge, Q. et al. Structural characterization of a unique interface between carbohydrate response element-binding protein (ChREBP) and 14-3-3beta protein. *J. Biol. Chem.* **287**, 41914–41921 (2012).
65. Stoltzman, C. A. et al. Glucose sensing by MondoA:Mlx complexes: a role for hexokinases and direct regulation of thioredoxin-interacting protein expression. *Proc. Natl Acad. Sci. USA* **105**, 6912–6917 (2008).

66. Velazquez-Campoy, A., Ohtaka, H., Nezami, A., Muzammil, S. & Freire, E. Isothermal titration calorimetry. *Curr. Protoc. Cell Biol.* https://doi.org/10.1002/0471143030.cb1708s23 (2004).
67. Tiwari, V. et al. Glycerol-3-phosphate activates ChREBP, FGF21 transcription and lipogenesis in citrin deficiency. Preprint at *bioRxiv* https://doi.org/10.1101/2024.12.27.630525 (2025).
68. Cheong, M. C. et al. Ethanol induction of FGF21 in the liver is dependent on histone acetylation and ligand activation of ChREBP by glycerol-3-phosphate. *Proc. Natl Acad. Sci. USA* **122**, e2505263122 (2025).
69. Randle, P. J., Garland, P. B., Hales, C. N. & Newsholme, E. A. The glucose fatty-acid cycle. Its role in insulin sensitivity and the metabolic disturbances of diabetes mellitus. *Lancet* **1**, 785–789 (1963).
70. Kennedy, E. P. Biosynthesis of complex lipids. *Fed. Proc.* **20**, 934–940 (1961).
71. Hue, L. & Taegtmeyer, H. The Randle cycle revisited: a new head for an old hat. *Am. J. Physiol. Endocrinol. Metab.* **297**, E578–E591 (2009).
72. McGarry, J. D., Leatherman, G. F. & Foster, D. W. Carnitine palmitoyltransferase I. The site of inhibition of hepatic fatty acid oxidation by malonyl-CoA. *J. Biol. Chem.* **253**, 4128–4136 (1978).
73. Softic, S., Cohen, D. E. & Kahn, C. R. Role of dietary fructose and hepatic de novo lipogenesis in fatty liver disease. *Dig. Dis. Sci.* **61**, 1282–1293 (2016).
74. Ouyang, S. et al. Glycerol kinase drives hepatic de novo lipogenesis and triglyceride synthesis in nonalcoholic fatty liver by activating SREBP-1c transcription, upregulating DGAT1/2 expression, and promoting glycerol metabolism. *Adv. Sci.* https://doi.org/10.1002/advs.202401311 (2024).
75. Costa-Mattioli, M. & Walter, P. The integrated stress response: from mechanism to disease. *Science* https://doi.org/10.1126/science.aat5314 (2020).
76. Khan, M. S. H. et al. FGF21 acts in the brain to drive macronutrient-specific changes in behavioral motivation and brain reward signaling. *Mol. Metab.* **91**, 102068 (2024).
77. de la Ballina, L. R. et al. Amino acid transport associated to cluster of differentiation 98 heavy chain (CD98hc) is at the cross-road of oxidative stress and amino acid availability. *J. Biol. Chem.* **291**, 9700–9711 (2016).
78. Lomelino, C. L., Andring, J. T., McKenna, R. & Kilberg, M. S. Asparagine synthetase: function, structure, and role in disease. *J. Biol. Chem.* **292**, 19952–19958 (2017).
79. Kraus, J. P. et al. Cystathionine γ-lyase: clinical, metabolic, genetic, and structural studies. *Mol. Genet. Metab.* **97**, 250–259 (2009).
80. Nikkanen, J. et al. Mitochondrial DNA replication defects disturb cellular dNTP pools and remodel one-carbon metabolism. *Cell Metab.* **23**, 635–648 (2016).
81. Mick, E. et al. Distinct mitochondrial defects trigger the integrated stress response depending on the metabolic state of the cell. *Elife* https://doi.org/10.7554/eLife.49178 (2020).
82. Dong, J., Qiu, H., Garcia-Barrio, M., Anderson, J. & Hinnebusch, A. G. Uncharged tRNA activates GCN2 by displacing the protein kinase moiety from a bipartite tRNA-binding domain. *Mol. Cell* **6**, 269–279 (2000).
83. Watatani, Y. et al. Stress-induced translation of ATF5 mRNA is regulated by the 5′-untranslated region. *J. Biol. Chem.* **283**, 2543–2553 (2008).
84. Lee, J. I. et al. HepG2/C3A cells respond to cysteine deprivation by induction of the amino acid deprivation/integrated stress response pathway. *Physiol. Genom.* **33**, 218–229 (2008).
85. Birsoy, K. et al. An essential role of the mitochondrial electron transport chain in cell proliferation is to enable aspartate synthesis. *Cell* **162**, 540–551 (2015).
86. Gudmundsson, S. et al. Variant interpretation using population databases: lessons from gnomAD. *Hum. Mutat.* **43**, 1012–1030 (2022).
87. Sakaue, S. et al. A cross-population atlas of genetic associations for 220 human phenotypes. *Nat. Genet.* **53**, 1415–1424 (2021).
88. Costanzo, M. C. et al. The Type 2 Diabetes Knowledge Portal: an open access genetic resource dedicated to type 2 diabetes and related traits. *Cell Metab.* **35**, 695–710 e696 (2023).
89. Larsson, S. C., Michaelsson, K., Mola-Caminal, M., Hoijer, J. & Mantzoros, C. S. Genome-wide association and Mendelian randomization study of fibroblast growth factor 21 reveals causal associations with hyperlipidemia and possibly NASH. *Metabolism* **137**, 155329 (2022).
90. Turner, T. et al. FGF21 increases water intake, urine output and blood pressure in rats. *PLoS ONE* **13**, e0202182 (2018).
91. Giontella, A. et al. Renoprotective effects of genetically proxied fibroblast growth factor 21: Mendelian randomization, proteome-wide and metabolome-wide association study. *Metabolism* **145**, 155616 (2023).
92. Frayling, T. M. et al. A common allele in FGF21 associated with sugar intake is associated with body shape, lower total body-fat percentage, and higher blood pressure. *Cell Rep.* **23**, 327–336 (2018).
93. May-Wilson, S. et al. Large-scale GWAS of food liking reveals genetic determinants and genetic correlations with distinct neurophysiological traits. *Nat. Commun.* **13**, 2743 (2022).
94. Liang, K. Mitochondrial CPT1A: insights into structure, function, and basis for drug development. *Front Pharm.* **14**, 1160440 (2023).
95. Srivastava, R. A. et al. AMP-activated protein kinase: an emerging drug target to regulate imbalances in lipid and carbohydrate metabolism to treat cardio-metabolic diseases. *J. Lipid Res.* **53**, 2490–2514 (2012).
96. Yang, R., Xu, A. & Kharitonenkov, A. Another kid on the block: long-acting FGF21 analogue to treat dyslipidemia and fatty liver. *J. Clin. Endocrinol. Metab.* **107**, e417–e419 (2022).
97. Gilroy, C. A. et al. Sustained release of a GLP-1 and FGF21 dual agonist from an injectable depot protects mice from obesity and hyperglycemia. *Sci. Adv.* **6**, eaaz9890 (2020).
98. Trammell, S. A. et al. Nicotinamide riboside is uniquely and orally bioavailable in mice and humans. *Nat. Commun.* **7**, 12948 (2016).
99. Trammell, S. A. et al. Nicotinamide riboside opposes type 2 diabetes and neuropathy in mice. *Sci. Rep.* **6**, 26933 (2016).
100. Bolger, A. M., Lohse, M. & Usadel, B. Trimmomatic: a flexible trimmer for Illumina sequence data. *Bioinformatics* **30**, 2114–2120 (2014).
101. Chen, S., Zhou, Y., Chen, Y. & Gu, J. fastp: an ultra-fast all-in-one FASTQ preprocessor. *Bioinformatics* **34**, i884–i890 (2018).
102. Dobin, A. et al. STAR: ultrafast universal RNA-seq aligner. *Bioinformatics* **29**, 15–21 (2013).
103. Anders, S. & Huber, W. Differential expression analysis for sequence count data. *Genome Biol.* **11**, R106 (2010).
104. Robinson, M. D., McCarthy, D. J. & Smyth, G. K. edgeR: a Bioconductor package for differential expression analysis of digital gene expression data. *Bioinformatics* **26**, 139–140 (2010).
105. McCarthy, D. J., Chen, Y. & Smyth, G. K. Differential expression analysis of multifactor RNA-Seq experiments with respect to biological variation. *Nucleic Acids Res.* **40**, 4288–4297 (2012).
106. Trammell, S. A. & Brenner, C. Targeted, LCMS-based metabolomics for quantitative measurement of NAD(+) metabolites. *Comput. Struct. Biotechnol. J.* https://doi.org/10.5936/csbj.201301012 (2013).
107. Sillero, M. A., Sillero, A. & Sols, A. Enzymes involved in fructose metabolism in liver and the glyceraldehyde metabolic crossroads. *Eur. J. Biochem.* **10**, 345–350 (1969).

Acknowledgements
We thank T. Saheki (Kumamoto University) and the Citrin Foundation for introduction to the problem of CD and for donation of *Slc25a13*$^{-/-}$*Gpd2*$^{-/-}$ mouse sperm, W. Tsark at City of Hope for in vitro fertilization and T.-F. Chou at the Proteome Exploration Laboratory of the California Institute of Technology for assistance with mass spectrometry. We thank P. Fueger, C. Mallet, J. Williams, Z. Wang, Y. Deng, S. Shuck and R. Natarajan for helpful consultations. This work was supported by National Institutes of Health grant nos. R01DK012170 and R01DK100425 (M.A.H.); National Institutes of Health grant nos. R01DK118011 and R01DK136671 (C.N.S.); American Diabetes Association grant no. 11-22-JDFPM-06 (C.N.S.); National Institutes of Health grant no. R01DK134675 (R.P.G.); Burroughs Wellcome Career Award for Medical Scientists (R.P.G.); National Institutes of Health grant no. R01HL147545 (C.B.); National Institutes of Health grant no. P30CA33572 (City of Hope shared resources); Alfred E. Mann Family Foundation and the Arthur Riggs Diabetes and Metabolism Research Institute (C.B.).

Author contributions
C.B. conceived of the project with M.A.H., C.N.S. and R.P.G., all of whom also provided funding. V.T., B.J., O.S., E.D.J.L.G., H.S., A.Z., C.N.S., R.P.G. and C.B. performed experiments and experimental analysis. M.-H.C. and X.W. performed data analysis. C.B. wrote and edited the manuscript with the assistance of all authors.

Competing interests
C.B. is the coinventor of US provisional patent application 63/739,033 for G3P-releasing prodrugs as FGF21-inducing compounds. The other authors declare no competing interests.

Additional information
Extended data is available for this paper at https://doi.org/10.1038/s42255-025-01399-3.

Supplementary information The online version contains supplementary material available at https://doi.org/10.1038/s42255-025-01399-3.

Correspondence and requests for materials should be addressed to Charles Brenner.

Peer review information *Nature Metabolism* thanks Araceli del Arco, Eleftheria Maratos-Flier and the other, anonymous, reviewer(s) for their contribution to the peer review of this work. Primary Handling Editor: Yanina-Yasmin Pesch, in collaboration with the *Nature Metabolism* team.

https://doi.org/10.1038/s42255-025-01399-3

Extended Data Table 1 | Hepatic gene expression (mean FPKM+/- SE) with NADH shuttle gene deletion and/or glycerol exposure

genotype	WT	WT	*Slc25a13-/-*	*Slc25a13-/-*	*Gpd2-/-*	*Gpd2-/-*	*Slc25a13-/- Gpd2 -/-*	*Slc25a13-/- Gpd2 -/-*
condition	water	glycerol	water	glycerol	water	glycerol	water	glycerol
n	4	5	7	7	4	5	4	4
mRNA								
ChREBPα	26.5 +/- 1.9	62.3 +/- 10.4	17.7 +/- 2.3	32.3 +/- 11.3	26.6 +/- 6.5	50.7 +/- 3.3	23.3 +/- 7.8	19.2 +/- 1.8
ChREBPβ	1.5 +/- 0.9	10.9 +/- 2.0	6.9 +/- 1.3	13.9 +/- 2.4	6.6 +/- 3.1	23.0 +/- 4.3	19.0 +/- 6.9	17.6 +/- 2.6
Fgf21	1.4 +/- 0.2	3.5 +/- 1.3	1.5 +/- 0.4	4.4 +/- 1.5	1.7 +/- 0.6	2.5 +/- 0.5	6.5 +/- 2.9	5.2 +/- 1.0
Srebf1	50.8 +/- 8.6	62.4 +/- 7.0	47.7 +/- 8.4	51.7 +/- 4.7	33.2 +/- 6.1	31.4 +/- 4.9	69.3 +/- 12.1	64.6 +/- 15.7

Liver gene expression levels (mean FPKM+/- SE) of select genes are reported across four genotypes of mice exposed to either two days of water or two days of 5% (w/v) glycerol. The data show that *ChREBPα, ChREBPβ* and *Fgf21* respond to NADH shuttle gene deletion and glycerol but that *Srebf1* does not respond to these conditions.

https://doi.org/10.1038/s42255-025-01399-3

Extended Data Table 2 | Most frequent pathological variants of *SLC25A13* in gnomAD (March 12, 2024)

RSID	Allele count	Origin
rs80338720	185	Asian
rs80338722	102	Asian
rs780525233	84	European
rs80338716	73	European
rs80338729	58	South Asian
rs200237622	56	Ashkenazi
rs80338721	32	European
rs80338725	30	Asian
rs781452100	30	European
rs80338723	23	Asian
rs143181462	22	European

nature portfolio

Corresponding author(s): Charles Brenner

Last updated by author(s): Charles Brenner

Reporting Summary

Nature Portfolio wishes to improve the reproducibility of the work that we publish. This form provides structure for consistency and transparency in reporting. For further information on Nature Portfolio policies, see our Editorial Policies and the Editorial Policy Checklist.

Please do not complete any field with "not applicable" or n/a. Refer to the help text for what text to use if an item is not relevant to your study.
For final submission: please carefully check your responses for accuracy; you will not be able to make changes later.

Statistics

For all statistical analyses, confirm that the following items are present in the figure legend, table legend, main text, or Methods section.

n/a	Confirmed	
☐	☑	The exact sample size (*n*) for each experimental group/condition, given as a discrete number and unit of measurement
☐	☑	A statement on whether measurements were taken from distinct samples or whether the same sample was measured repeatedly
☐	☑	The statistical test(s) used AND whether they are one- or two-sided *Only common tests should be described solely by name; describe more complex techniques in the Methods section.*
☑	☐	A description of all covariates tested
☐	☑	A description of any assumptions or corrections, such as tests of normality and adjustment for multiple comparisons
☐	☑	A full description of the statistical parameters including central tendency (e.g. means) or other basic estimates (e.g. regression coefficient) AND variation (e.g. standard deviation) or associated estimates of uncertainty (e.g. confidence intervals)
☐	☑	For null hypothesis testing, the test statistic (e.g. *F*, *t*, *r*) with confidence intervals, effect sizes, degrees of freedom and *P* value noted *Give P values as exact values whenever suitable.*
☐	☑	For Bayesian analysis, information on the choice of priors and Markov chain Monte Carlo settings
☑	☐	For hierarchical and complex designs, identification of the appropriate level for tests and full reporting of outcomes
☑	☐	Estimates of effect sizes (e.g. Cohen's *d*, Pearson's *r*), indicating how they were calculated

Our web collection on statistics for biologists contains articles on many of the points above.

Software and code

Policy information about availability of computer code

Data collection: all methods disclosed

Data analysis: all software disclosed and cited

For manuscripts utilizing custom algorithms or software that are central to the research but not yet described in published literature, software must be made available to editors and reviewers. We strongly encourage code deposition in a community repository (e.g. GitHub). See the Nature Portfolio guidelines for submitting code & software for further information.

Data

Policy information about availability of data

All manuscripts must include a data availability statement. This statement should provide the following information, where applicable:

- Accession codes, unique identifiers, or web links for publicly available datasets
- A description of any restrictions on data availability
- For clinical datasets or third party data, please ensure that the statement adheres to our policy

Research involving human participants, their data, or biological material

Policy information about studies with human participants or human data. See also policy information about sex, gender (identity/presentation), and sexual orientation and race, ethnicity and racism.

Reporting on sex and gender	
Reporting on race, ethnicity, or other socially relevant groupings	
Population characteristics	
Recruitment	
Ethics oversight	

Note that full information on the approval of the study protocol must also be provided in the manuscript.

Field-specific reporting

Please select the one below that is the best fit for your research. If you are not sure, read the appropriate sections before making your selection.

☑ Life sciences ☐ Behavioural & social sciences ☐ Ecological, evolutionary & environmental sciences

For a reference copy of the document with all sections, see nature.com/documents/nr-reporting-summary-flat.pdf

Life sciences study design

All studies must disclose on these points even when the disclosure is negative.

Sample size	disclosed
Data exclusions	disclosed
Replication	disclosed
Randomization	disclosed
Blinding	disclosed

Behavioural & social sciences study design

All studies must disclose on these points even when the disclosure is negative.

Study description	n/a
Research sample	
Sampling strategy	
Data collection	
Timing	
Data exclusions	
Non-participation	
Randomization	

Ecological, evolutionary & environmental sciences study design

All studies must disclose on these points even when the disclosure is negative.

Study description	n/a
Research sample	
Sampling strategy	
Data collection	
Timing and spatial scale	
Data exclusions	
Reproducibility	
Randomization	
Blinding	

Did the study involve field work? ☐ Yes ☐ No

Field work, collection and transport

Field conditions	n/a
Location	
Access & import/export	
Disturbance	

Reporting for specific materials, systems and methods

We require information from authors about some types of materials, experimental systems and methods used in many studies. Here, indicate whether each material, system or method listed is relevant to your study. If you are not sure if a list item applies to your research, read the appropriate section before selecting a response.

Materials & experimental systems

n/a	Involved in the study
☐	☑ Antibodies
☐	☑ Eukaryotic cell lines
☑	☐ Palaeontology and archaeology
☐	☑ Animals and other organisms
☐	☑ Clinical data
☑	☐ Dual use research of concern
☑	☐ Plants

Methods

n/a	Involved in the study
☑	☐ ChIP-seq
☑	☐ Flow cytometry
☑	☐ MRI-based neuroimaging

Antibodies

Antibodies used	FGF21 ELISA Cat. No. MF2100
Validation	manufacturer citations and data

Eukaryotic cell lines

Policy information about cell lines and Sex and Gender in Research

Cell line source(s)	HEK-293T
Authentication	ATCC
Mycoplasma contamination	none
Commonly misidentified lines (See ICLAC register)	n/a

Palaeontology and Archaeology

Specimen provenance	n/a
Specimen deposition	
Dating methods	

☐ Tick this box to confirm that the raw and calibrated dates are available in the paper or in Supplementary Information.

Ethics oversight	

Note that full information on the approval of the study protocol must also be provided in the manuscript.

Animals and other research organisms

Policy information about studies involving animals; ARRIVE guidelines recommended for reporting animal research, and Sex and Gender in Research

Laboratory animals	all data provided
Wild animals	none
Reporting on sex	data provided
Field-collected samples	n/a
Ethics oversight	Approved by City of Hope IACUC and Institutional Biosafety Committee.

Note that full information on the approval of the study protocol must also be provided in the manuscript.

Clinical data

Policy information about clinical studies

All manuscripts should comply with the ICMJE guidelines for publication of clinical research and a completed CONSORT checklist must be included with all submissions.

Clinical trial registration	n/a
Study protocol	n/a
Data collection	n/a
Outcomes	n/a

Dual use research of concern

Policy information about dual use research of concern

Hazards

Could the accidental, deliberate or reckless misuse of agents or technologies generated in the work, or the application of information presented in the manuscript, pose a threat to:

No	Yes	
☑	☐	Public health
☑	☐	National security
☑	☐	Crops and/or livestock
☑	☐	Ecosystems
☑	☐	Any other significant area

Experiments of concern

Does the work involve any of these experiments of concern:

No	Yes	
☑	☐	Demonstrate how to render a vaccine ineffective
☑	☐	Confer resistance to therapeutically useful antibiotics or antiviral agents
☑	☐	Enhance the virulence of a pathogen or render a nonpathogen virulent
☑	☐	Increase transmissibility of a pathogen
☑	☐	Alter the host range of a pathogen
☑	☐	Enable evasion of diagnostic/detection modalities
☑	☐	Enable the weaponization of a biological agent or toxin
☑	☐	Any other potentially harmful combination of experiments and agents

Plants

Seed stocks: n/a

Novel plant genotypes:

Authentication:

ChIP-seq

Data deposition

☐ Confirm that both raw and final processed data have been deposited in a public database such as GEO.

☐ Confirm that you have deposited or provided access to graph files (e.g. BED files) for the called peaks.

Data access links
May remain private before publication.

Files in database submission

Genome browser session
(e.g. UCSC)

Methodology

Replicates

Sequencing depth

Antibodies

Peak calling parameters

Data quality

Software

Flow Cytometry

Plots

Confirm that:

☐ The axis labels state the marker and fluorochrome used (e.g. CD4-FITC).

☐ The axis scales are clearly visible. Include numbers along axes only for bottom left plot of group (a 'group' is an analysis of identical markers).

☐ All plots are contour plots with outliers or pseudocolor plots.

☐ A numerical value for number of cells or percentage (with statistics) is provided.

Methodology

Sample preparation

Instrument

Software

Cell population abundance

Gating strategy

☐ Tick this box to confirm that a figure exemplifying the gating strategy is provided in the Supplementary Information.

Magnetic resonance imaging

Experimental design

Design type

Design specifications

Behavioral performance measures

Imaging type(s)

Field strength

Sequence & imaging parameters

Area of acquisition

Diffusion MRI ☐ Used ☐ Not used

Preprocessing

Preprocessing software

Normalization

Normalization template

Noise and artifact removal

Volume censoring

Statistical modeling & inference

Model type and settings

Effect(s) tested

Specify type of analysis: ☐ Whole brain ☐ ROI-based ☐ Both

Statistic type for inference

(See Eklund et al. 2016)

Correction

Models & analysis

n/a	Involved in the study
☐	☐ Functional and/or effective connectivity
☐	☐ Graph analysis
☐	☐ Multivariate modeling or predictive analysis

Functional and/or effective connectivity

Graph analysis

Multivariate modeling and predictive analysis